Tees and tissues in the problems of applied hydrodynamics: applications to cerebral and abdominal hemodynamics

Parshin D.V.[1,2] , Tikhvinsky D.V.[1,2], Merzhoeva L.R.[1], Kuianova I.O. [1,2], Lipovka A.I[1,2], Khe A.K. [1,2], Karpenko A.A.[1,3], Dubovoy A.V. [4], **Chupakhin A.P.**[1,2]

1- Novosibirsk State University
2-Lavrentyev Institute of Hydrodynamics SB RAS
3-Meshalkin National Medical Research Center
4- Federal Neurosurgical Center (Novosibirsk)

Tomsk, December Readings - 2021

Outline

- About the problem
- Idealized numerical approach (CA)
- Idealized numerical approach (AAA)
- Strain-Stress testing
- Fluorescence
- Conclusions

Bifurcations everywhere

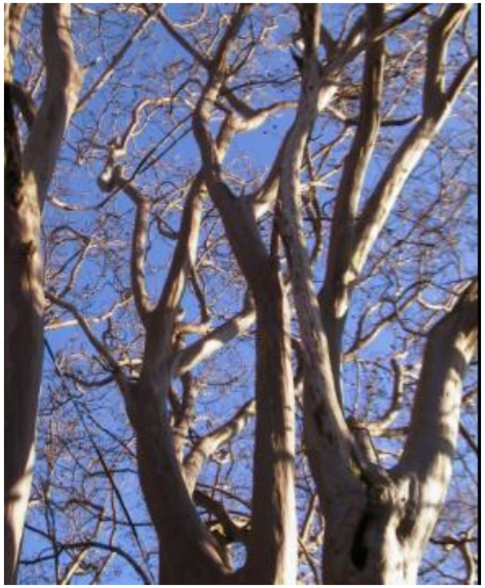

Trees

Rivers

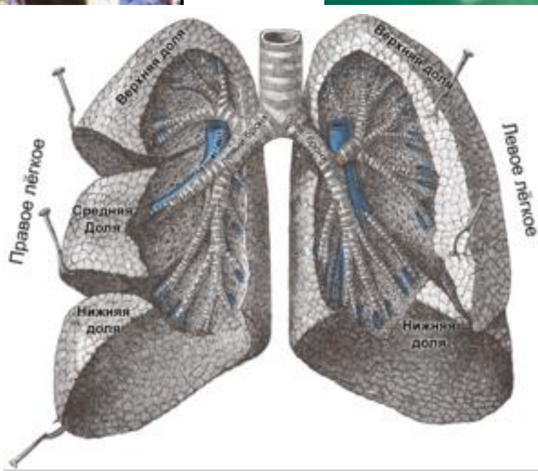

Organs

Blood vessels

Borrowed from
@https://evercare.ru/
@wiki
@freepics

Three-dimensional flow structures in X-shaped junctions: Effect of the Reynolds number and crossing angle

P. G. Correa, J. R. Mac Intyre, J. M. Gomba, M. A. Cachile, J. P. Hulin and H. Auradou

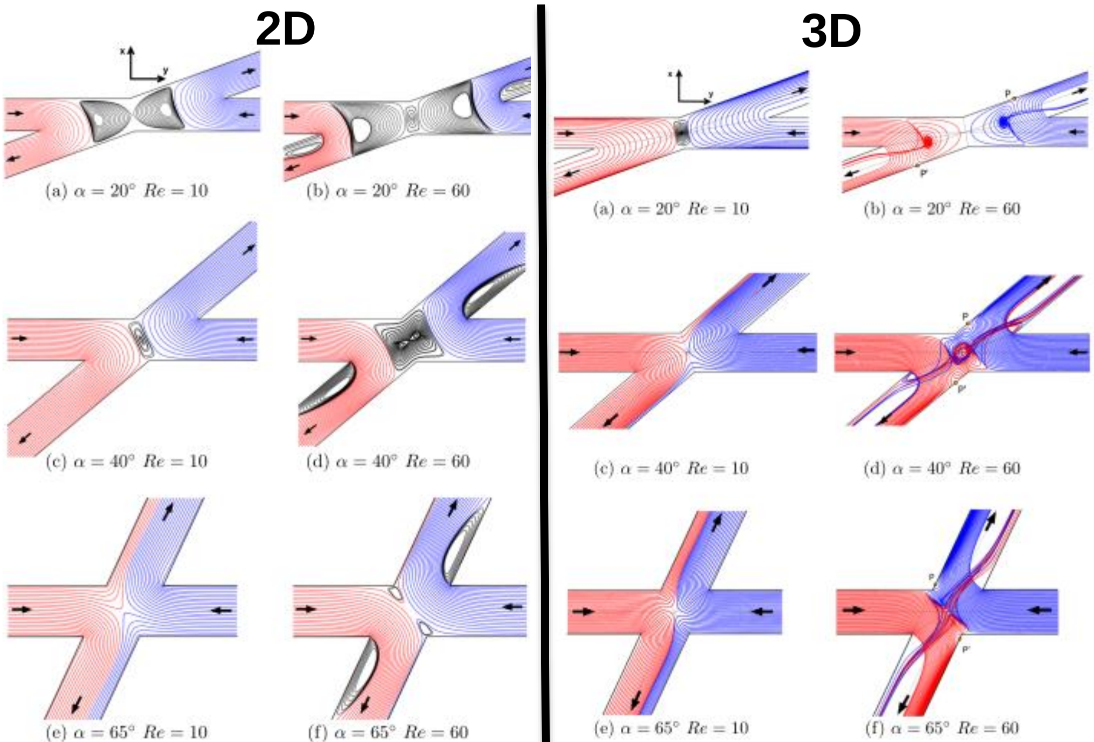

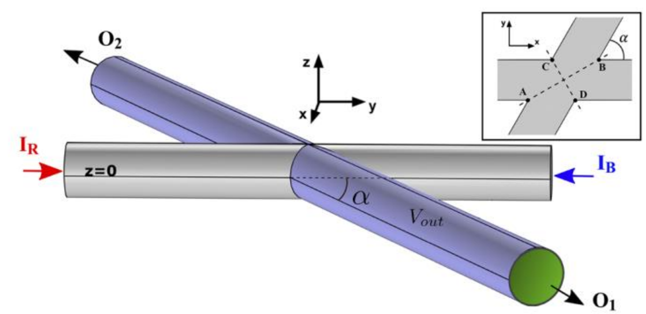

The present numerical study has characterized extensively the variations of the velocity and vorticity fields in X-shaped junctions with their angle α and the Reynolds number Re. Qualitative and quantitative comparison of 2D and 3D modeling.

DISCUSSION AND CONCLUSION

- Axial vortical structures of axis parallel to that of the outlet tubes, in addition to being only present in 3D simulations, appear only at large values of α and Re. A major characteristic of these structures is that they may strongly enhance the efficiency of mixing in the junctions
- These comparisons show therefore that while 2D simulations may provide simple models of physical transport mechanisms in junctions, they cannot make valid quantitative predictions even at low Reynolds numbers.

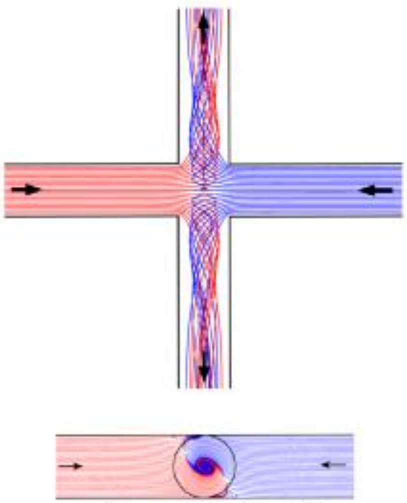

(b) $\alpha = 90°$ $Re = 60.$

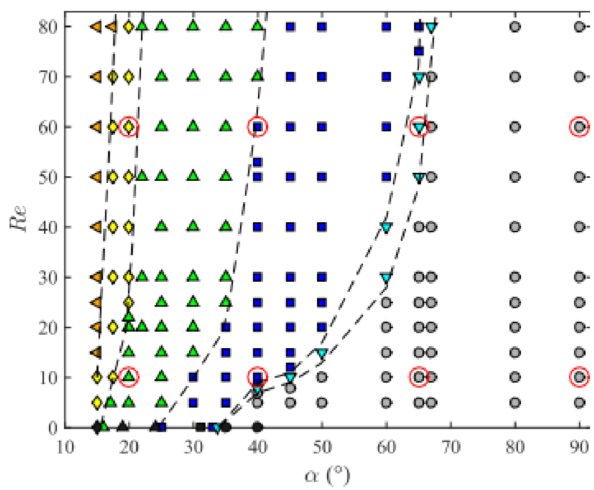

FIG. 7. 2D simulations. Map of the different flow configurations observed as a function of α vs Re. Symbols indicate the number of the vortices: gray filled circles, no vortex; navy blue filled squares, one vortex; green filled upward triangles, two vortices aligned along the major axis; blue filled downward triangles, two vortices aligned along the minor axis; yellow filled diamonds, three vortices; and orange filled left pointing triangles, four vortices. Red empty circles: cases presented in Figs. 2 and 3. Black symbols: results of Cachile *et al.* in the limit $Re \to 0$.

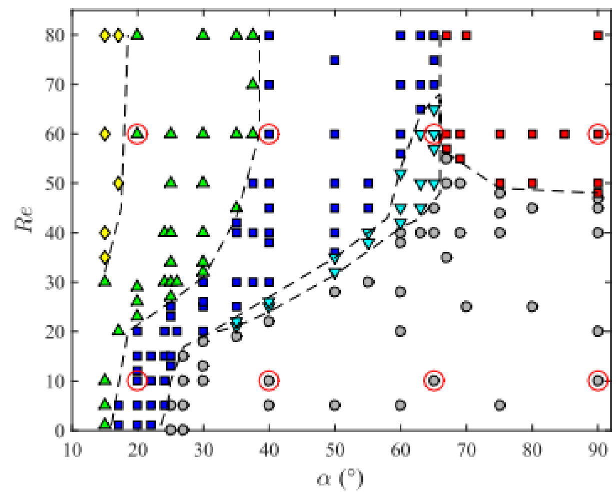

FIG. 8. 3D simulations. Map of the different flow configurations as a function of α vs Re. Symbols indicate the number and orientation of the vortices observed. Red filled squares: one vortex parallel to the axis of the outlet channels. Other symbols: vortices parallel to the z axis. Gray filled circles, no vortex; navy blue filled squares, one vortex; green filled upward triangles, two vortices; blue filled downward triangles, two vortices aligned along the minor axis; yellow filled diamonds, three vortices. Red empty circles: cases presented in Figs. 4–6.

Three-dimensional vortical structures and wall shear stress in a curved artery model

Christopher Cox, Mohammad Reza Najjari and Michael W. Plesniak

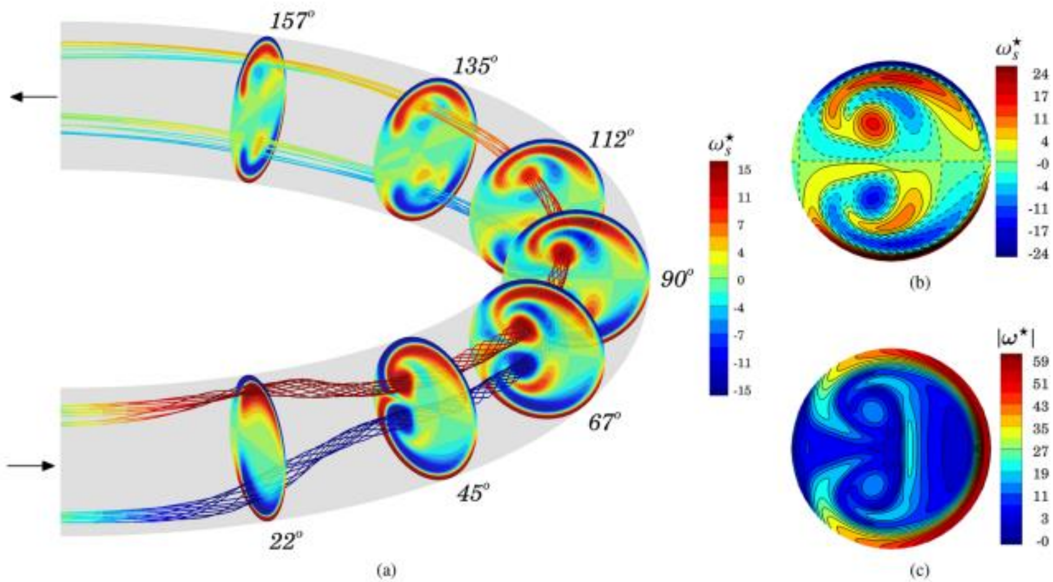

Presented distributions of instantaneous wall shear stress over the entire surface of the curve and concluded that a combination of intense secondary flow and flow reversal near the inner wall lead to local increases in wall shear stress

CONCLUSIONS

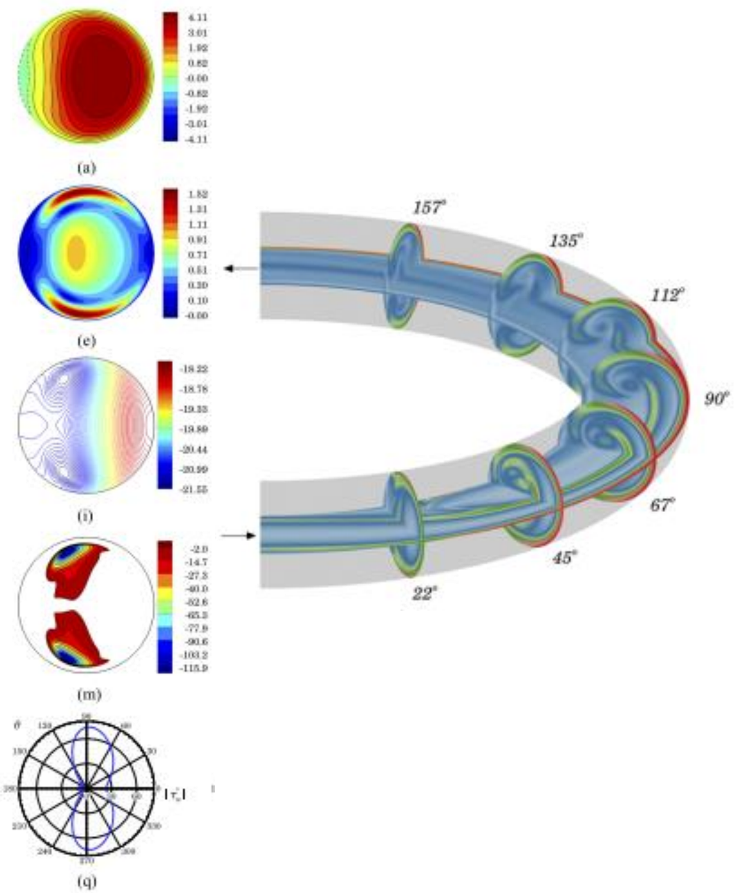

- Numerically investigated both spatial evolution and temporal evolution of multiple three-dimensional vortices under a fully developed physiological (pulsatile) inflow of a Newtonian blood analog fluid in a 180 , curved rigid pipe without taper or torsion—a simple model for a human artery with circular cross section and constant curvature.
- Qualitative and quantitative comparisons of numerical and experimental data were performed, and numerical results of secondary velocity and streamwise vorticity were shown to agree with experimental results captured via particle image velocimetry.
- Flow descriptions and trajectories of Dean-type (deformed Dean and split Dean) vortices were provided.
- Identified vortical structures using an appropriate vortex identification method and characterized their evolution throughout the deceleration phase of the physiologically relevant flow rate, capturing both Dean-type and Lyne-type vortices for which the planes of rotation are different.
- Connected downstream vorticity with the upstream Dean vortices.
- Presented distributions of instantaneous wall shear stress over the entire surface of the curve and concluded that a combination of intense secondary flow and flow reversal near the inner wall lead to local increases in wall shear stress.

Bypass surgery

- Cerebral bypass is a junction of cerebral
or cerebral-extracranial vessels to supp
necessary volume of blood flow rate.
- **Applications:**
  - Cerebral aneurysms
  - Intracranial stenosis
  - Tumors
  - Moya-moya disease
- Types of main bypass techniques:

1. Side-to-side
2. End-to-end
3. End-to-side

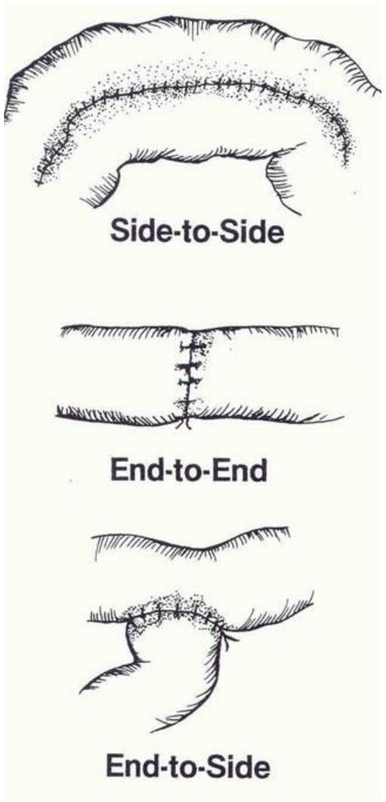

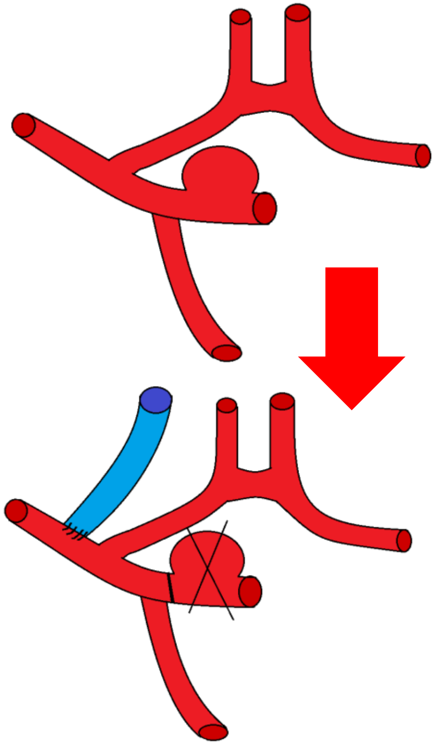

The technique of Bypass surgery

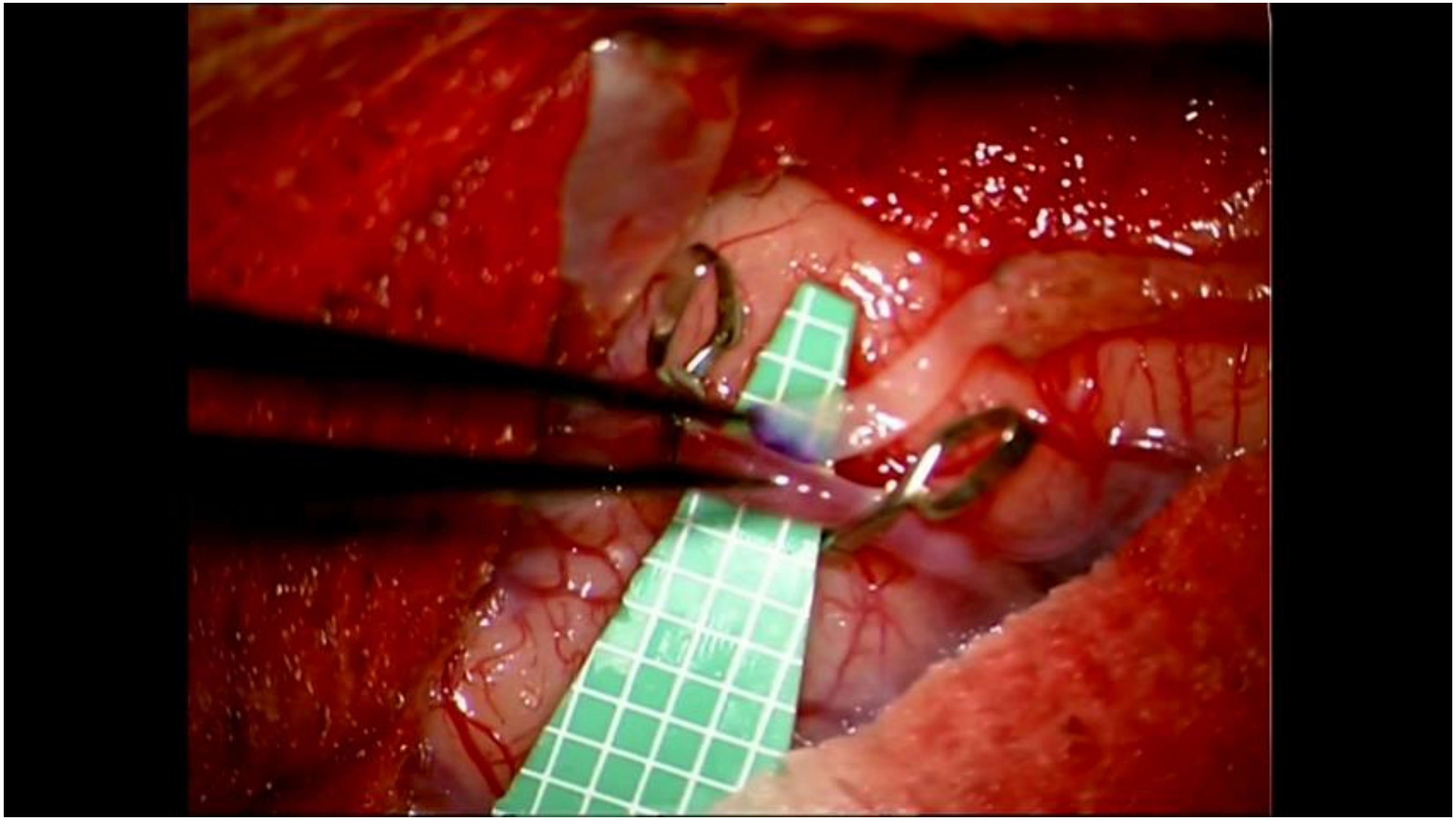

Federal Neurosurgical center (Novosibirsk), operating video

Abdominal aortic aneurysm (schematic view)

- AAA is a permanent focal dilation 50 percent greater than the normal diameter of the adjacent healthy aorta
- risk factors are associated with (mostly) age, male sex, being from a White population, a positive family history, smoking e.t.c.[1,2]

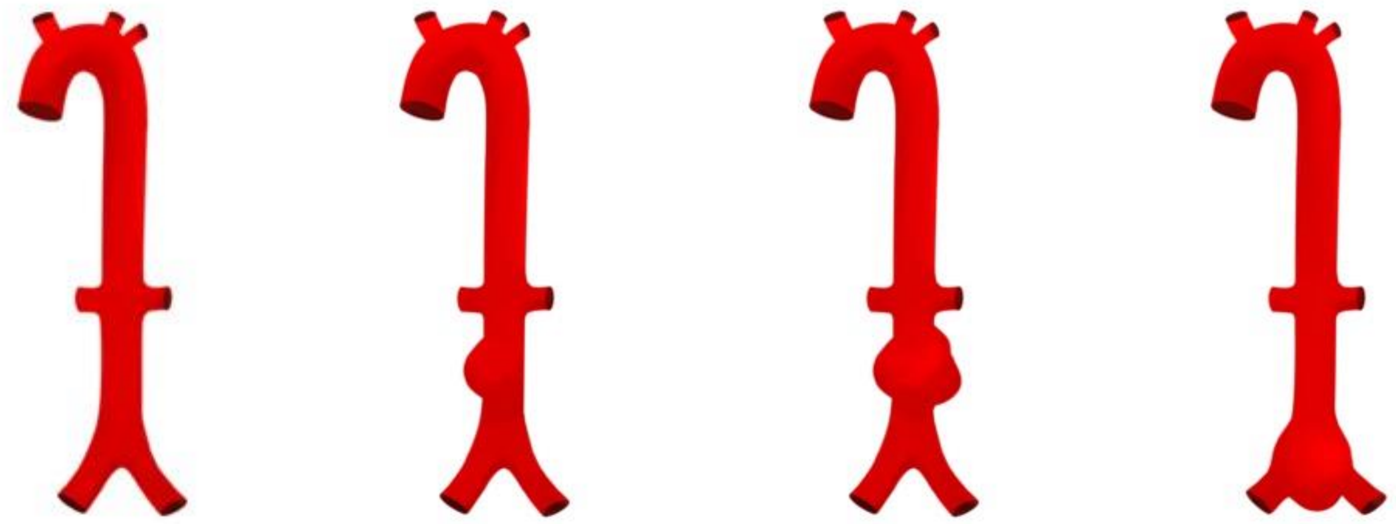

1. Chaikof EL, Dalman RL, Eskandari MK, et al. The Society for Vascular Surgery practice guidelines on the care of patients with an abdominal aortic aneurysm. J Vasc Surg 2018; 67:2.
2. Moll FL, Powell JT, Fraedrich G, et al. Management of abdominal aortic aneurysms clinical practice guidelines of the European society for vascular surgery. Eur J Vasc Endovasc Surg 2011; 41 Suppl 1:S1.

Idealized numerical setup

Azar D, et al, 2018

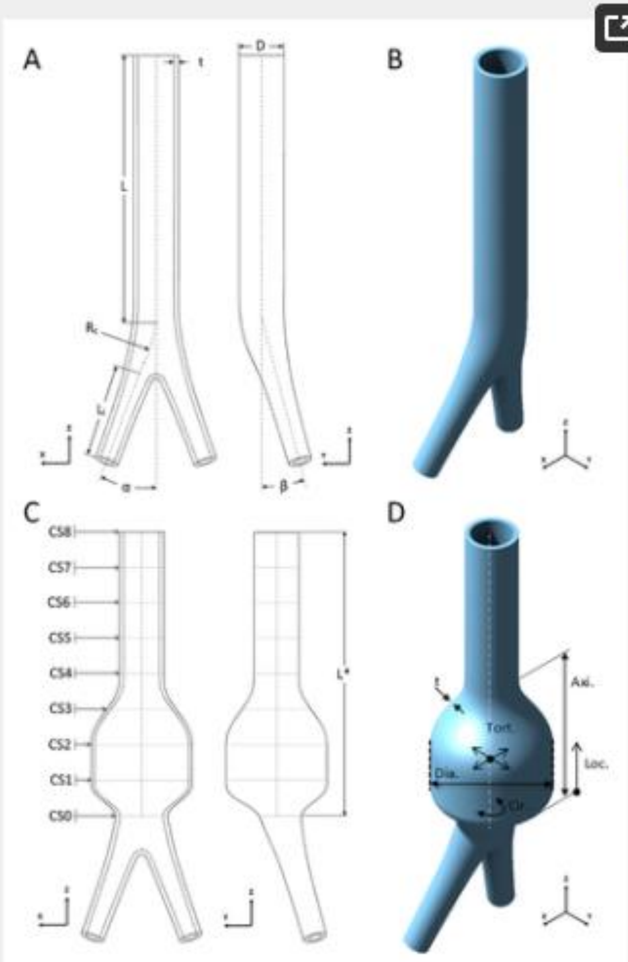

Download:

PPT PowerPoint slide

PNG larger image

TIFF original image

Fig 1. Referent normal aortic and baseline AAA geometries.

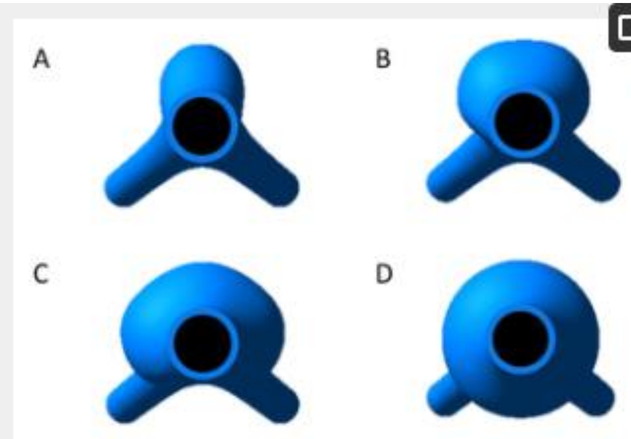

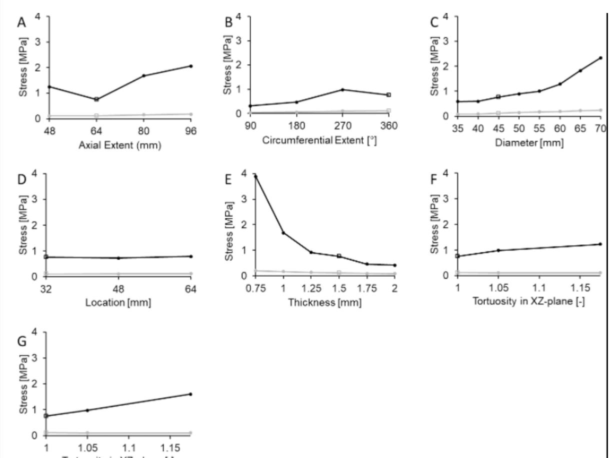

https://journals.plos.org/plosone/article?id=10.1371/journal.pone.0192032

Idealized numerical setup

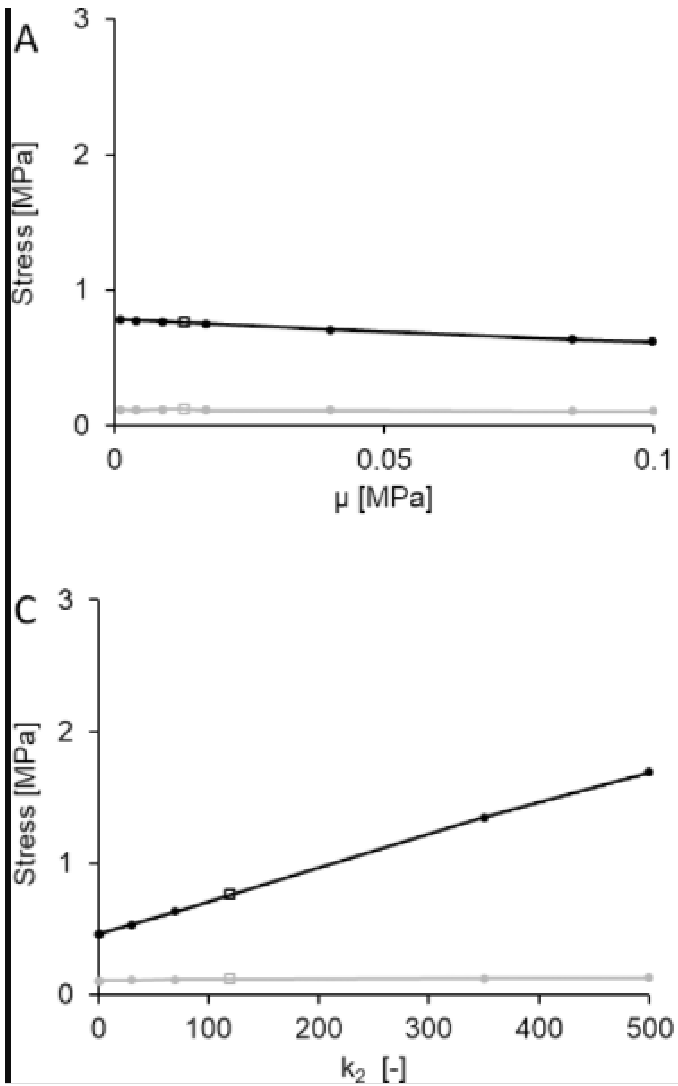

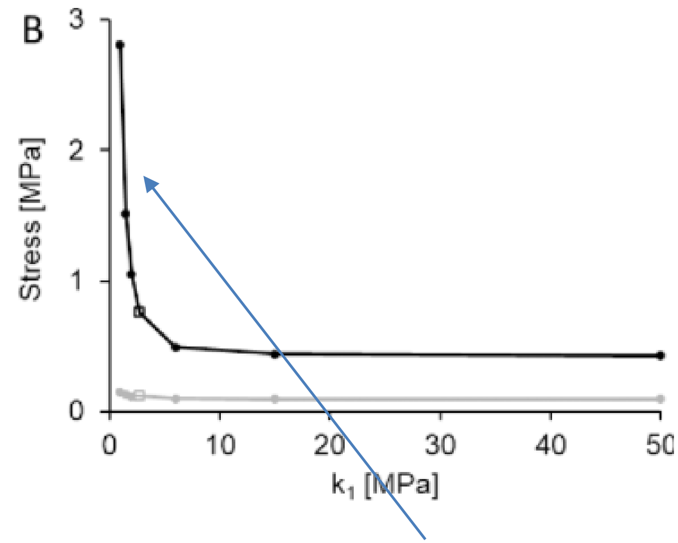

problems of idealized setup,
Ultimate stress becomes infinity due to the specific curvature value of the vessel surface

How daughter aneurysm (bleb) affects to the flow

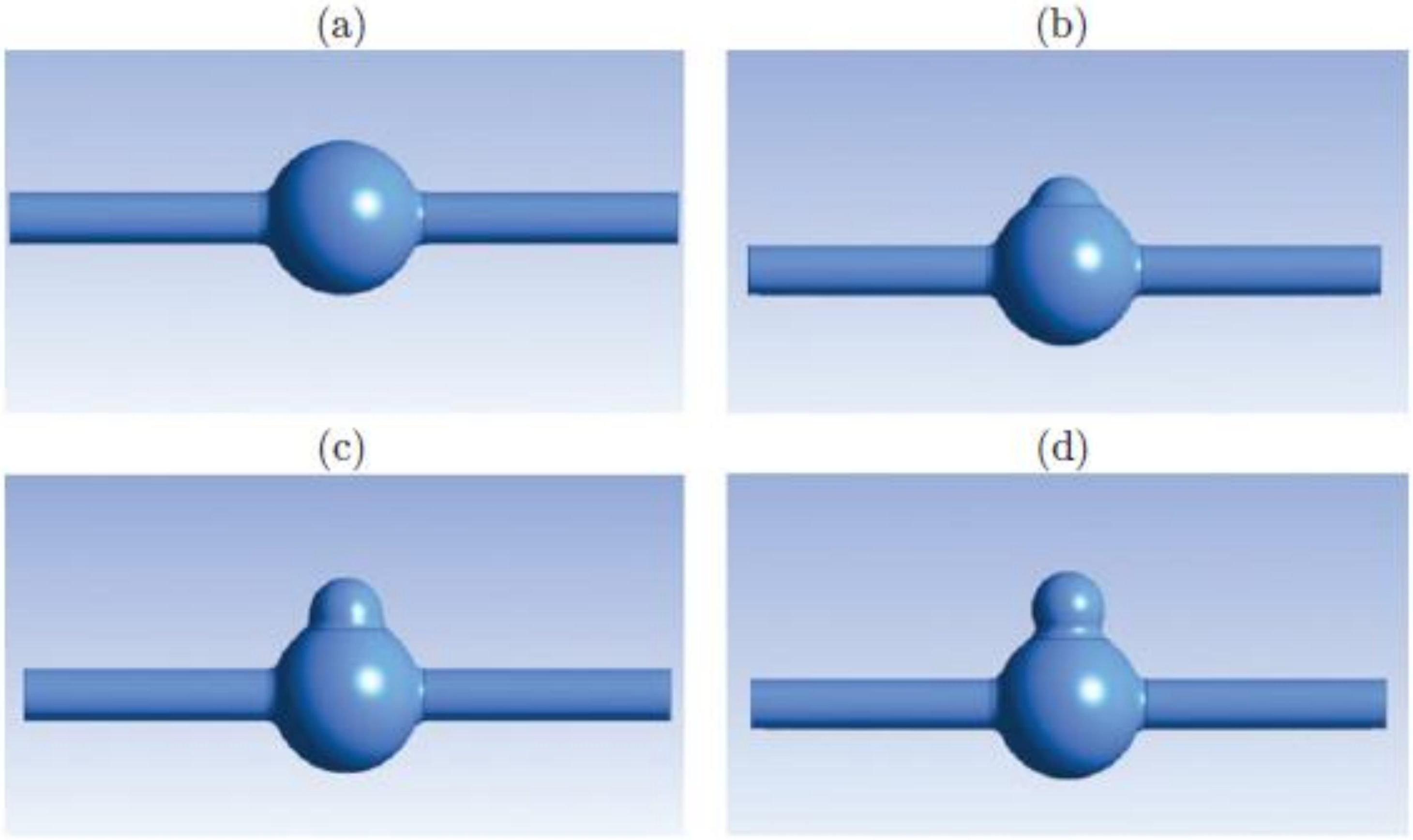

Fig. 2. Model configurations of aneurysms with a diverticulum of different height: $L = 0$ (a), $L = D/4$ (b), $L = D/2$ (c), and $L = 3D/4$ (d).

ENERGY CHARACTERISTICS OF THE HYDROELASTIC SYSTEM

$$E_{tot} = E_e + E_b + E_k,$$

$$E_e = \frac{Eh}{2(1-\nu^2)} \int_S dS;$$

$$E_b = \frac{Eh^3}{24(1-\nu^2)} \int_S H^2\, dS;$$

$$E_k = \frac{1}{2} \int_V \rho |\boldsymbol{v}|^2\, dV.$$

Here H is the mean curvature of the surface.

The presence of fluid viscosity leads to energy dissipation. The energy dissipated per unit time is given by the formula

$$E_v = 4\mu \int_V |\boldsymbol{\omega}|^2\, dV,$$

where $\boldsymbol{\omega} = \operatorname{rot} \boldsymbol{v}$. The flow energy for the model configurations was calculated in [34].

How bends affect to the flows, when we have an aneurysm and moreover daughter aneurysm (bleb)

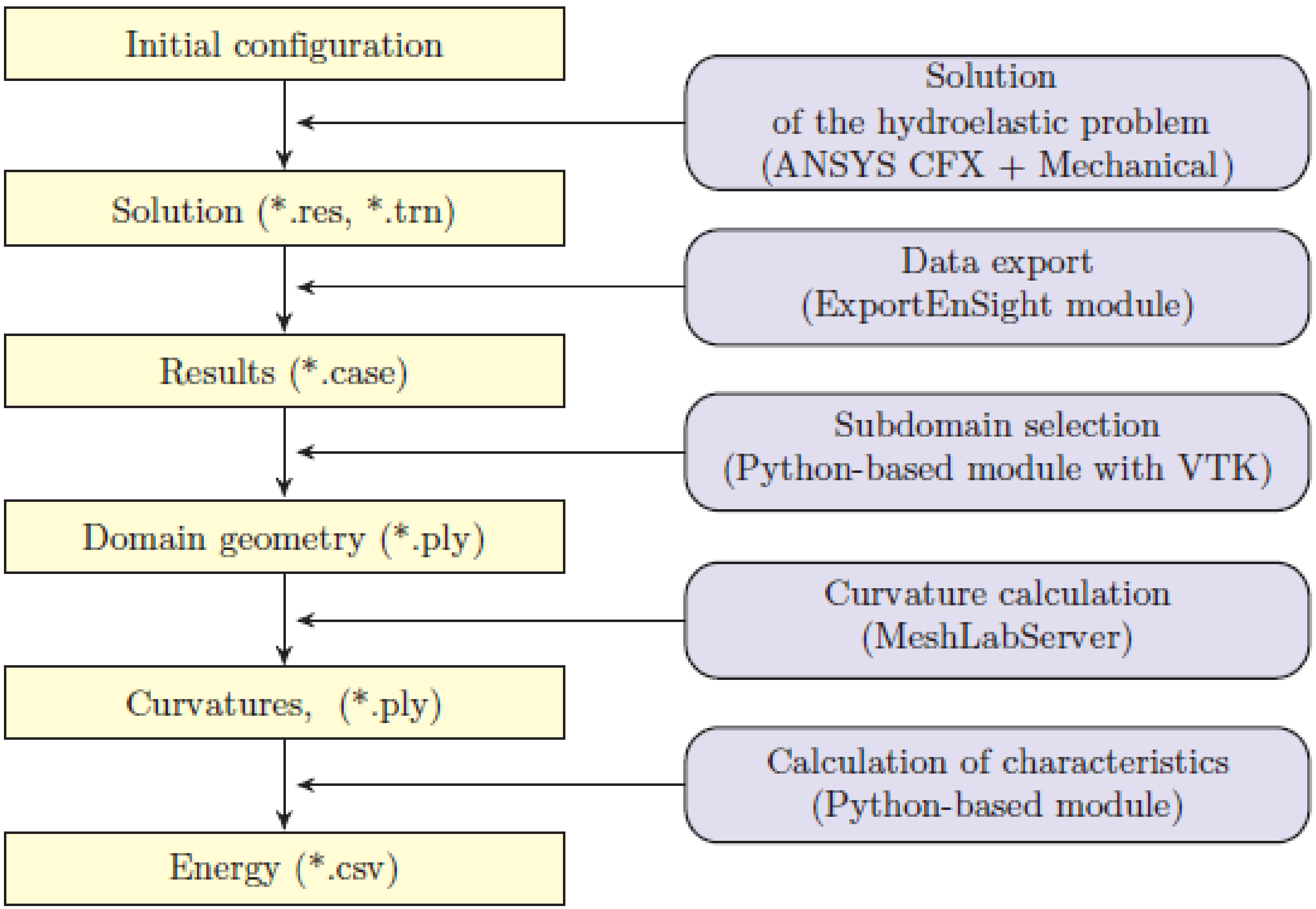

Results of the simulation

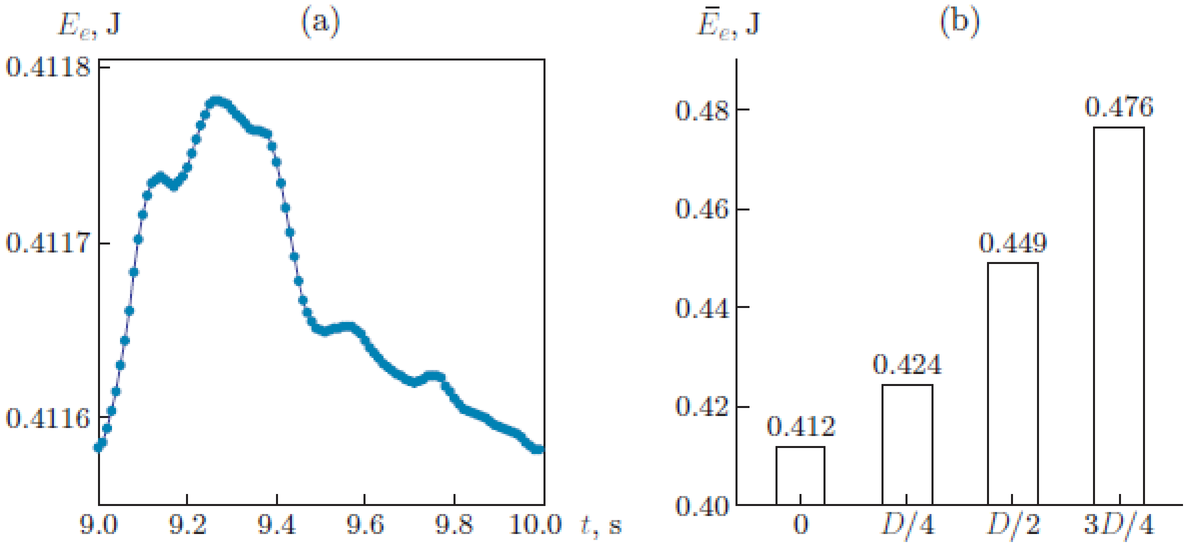

Elastic energy

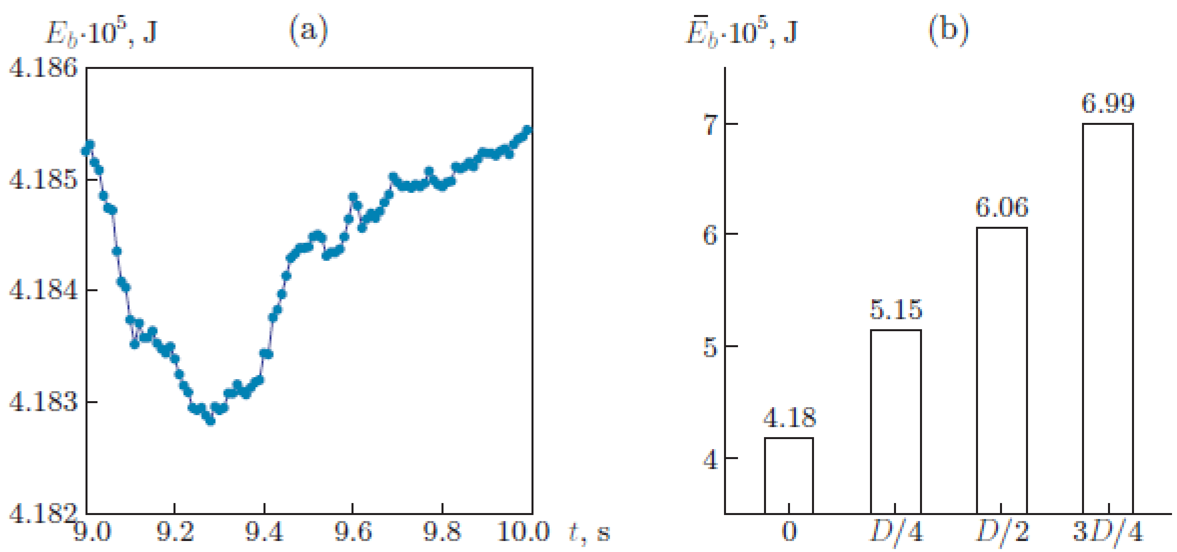

Bending energy

Results of the simulation

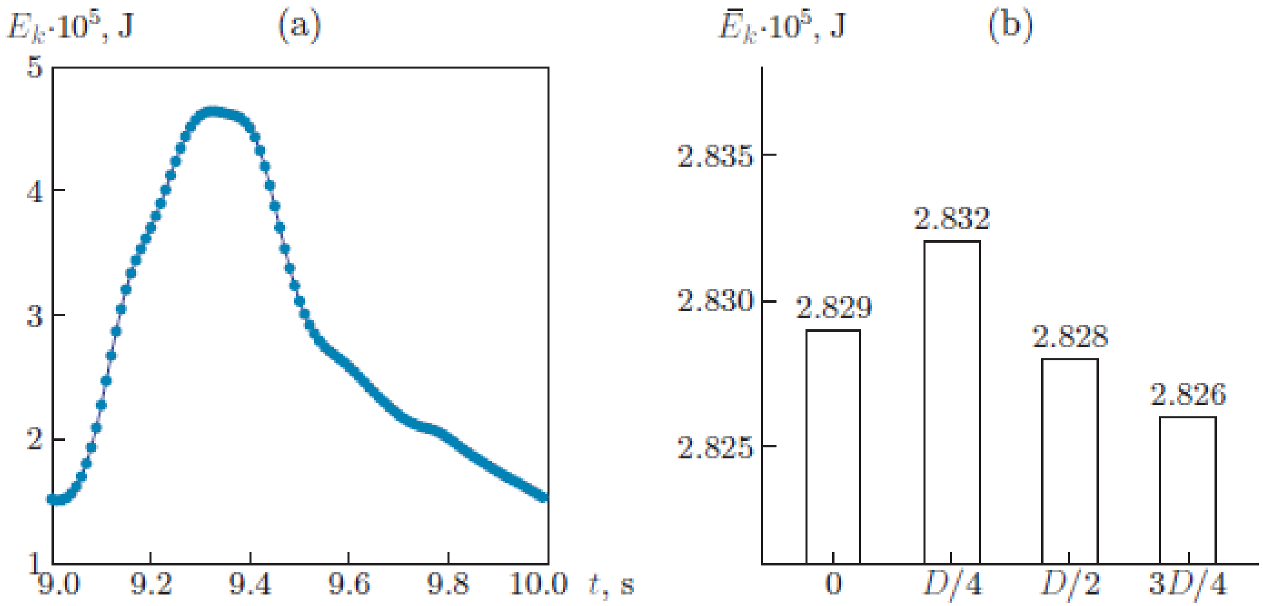

Kinetic energy

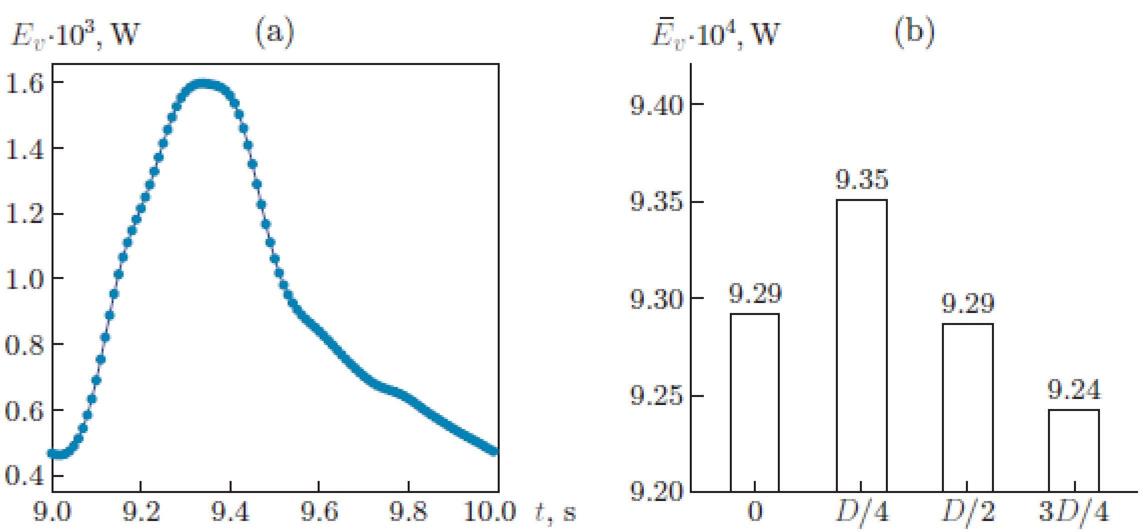

The power of viscous dissipation

The impact of each component

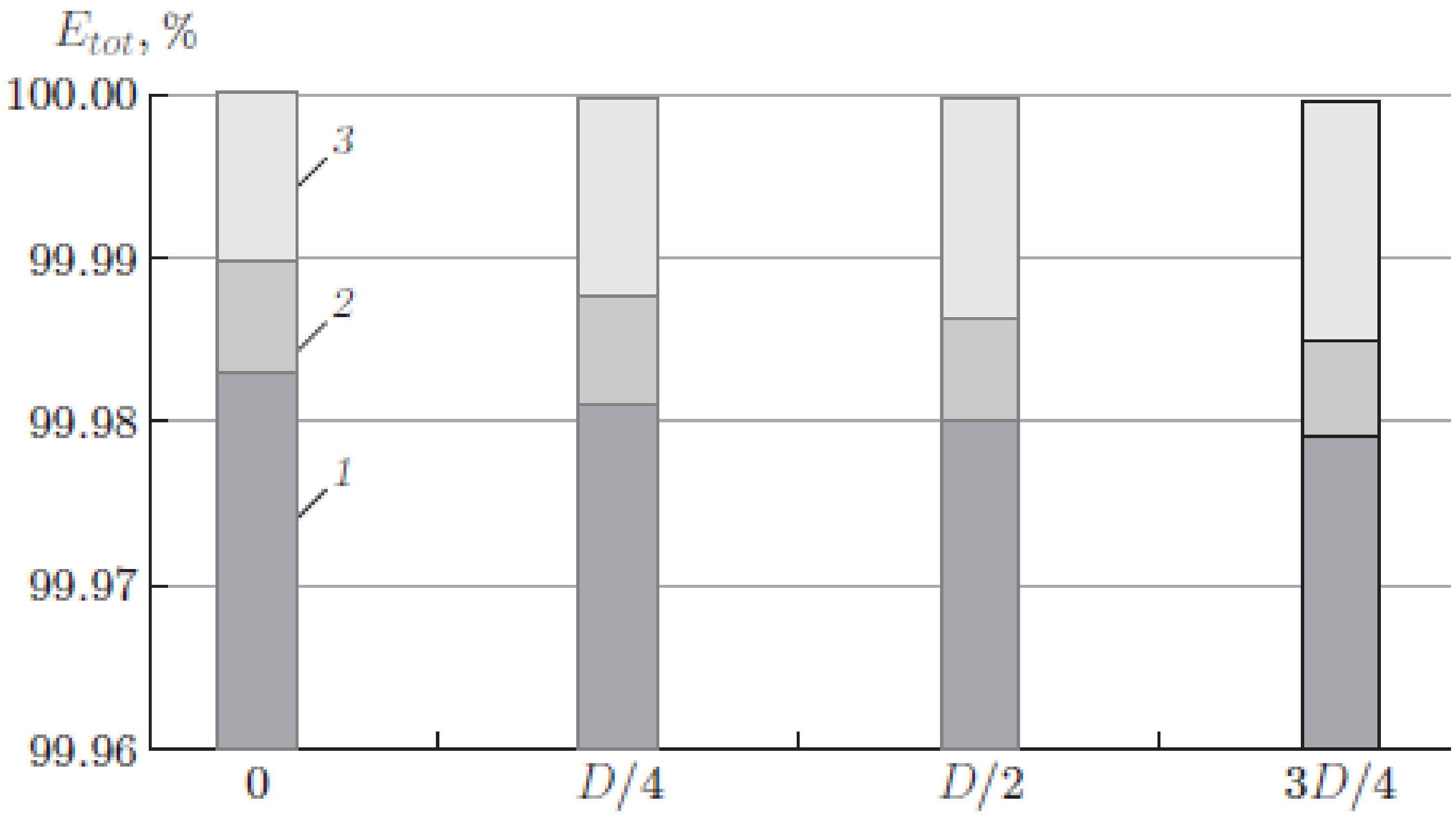

1- Elastic, 2 – Kinetic, 3- Bending

Patient specific time-distributed impact

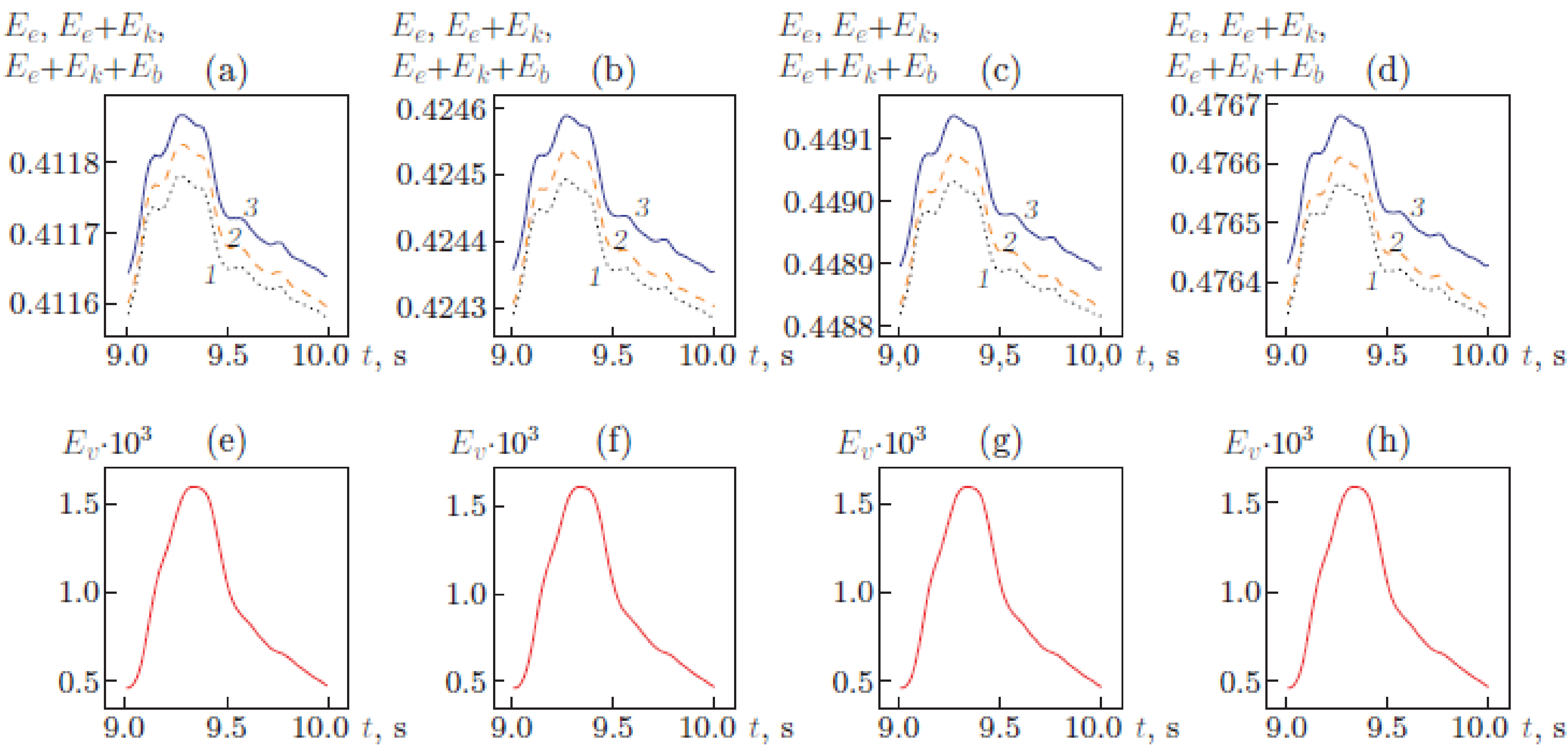

Velocity-Pressure diagrams

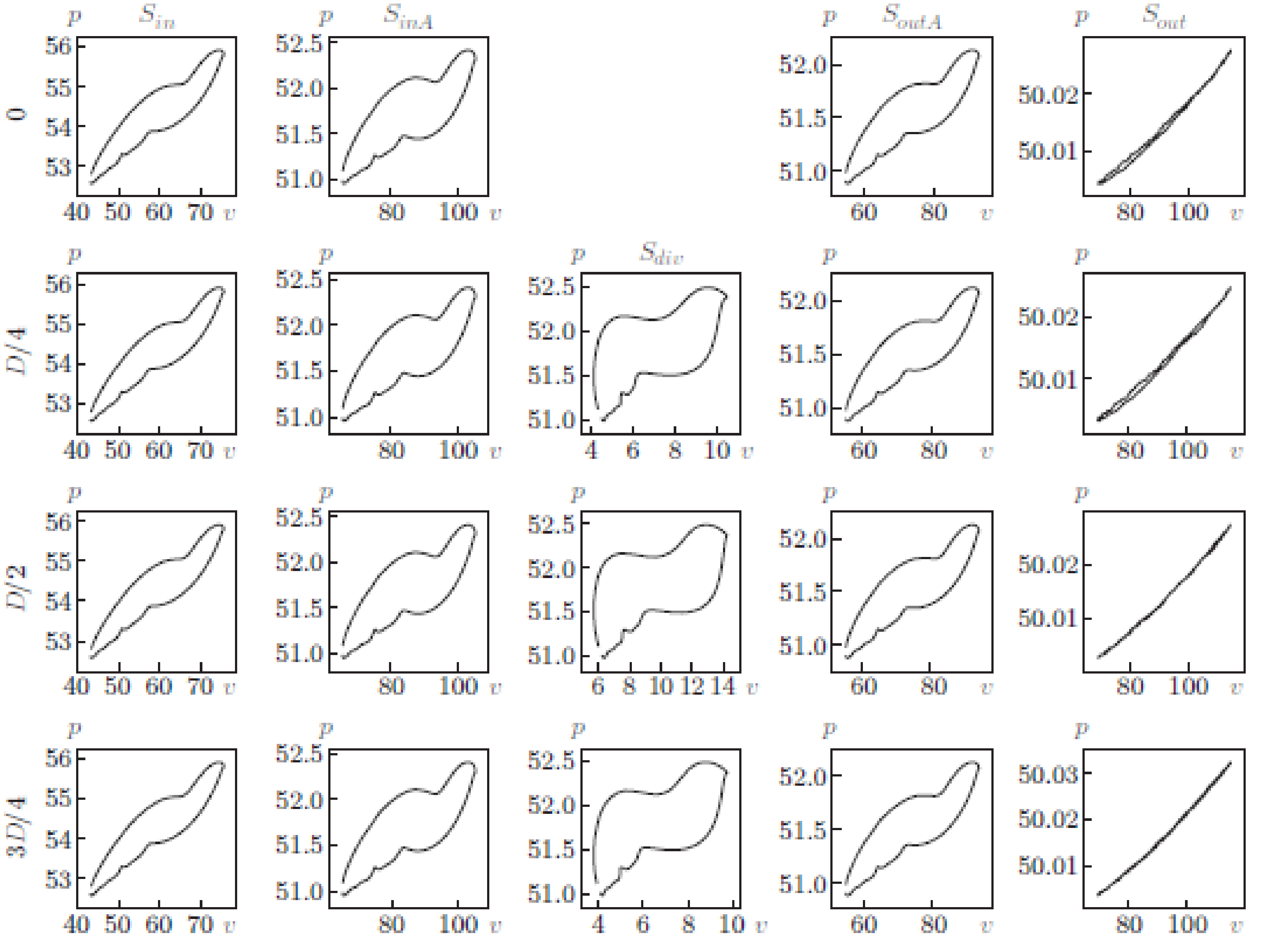

A. Khe et al, Applied mechanics and tech phys, 2020

How ideal constructions similar to real ones and what about the ‘laws’ ?

Patient-specific configurations (8 of 30 are presented) were analysed

Validation of a real patient-specific data with Murray's law (real aorta diameter vs expected one)

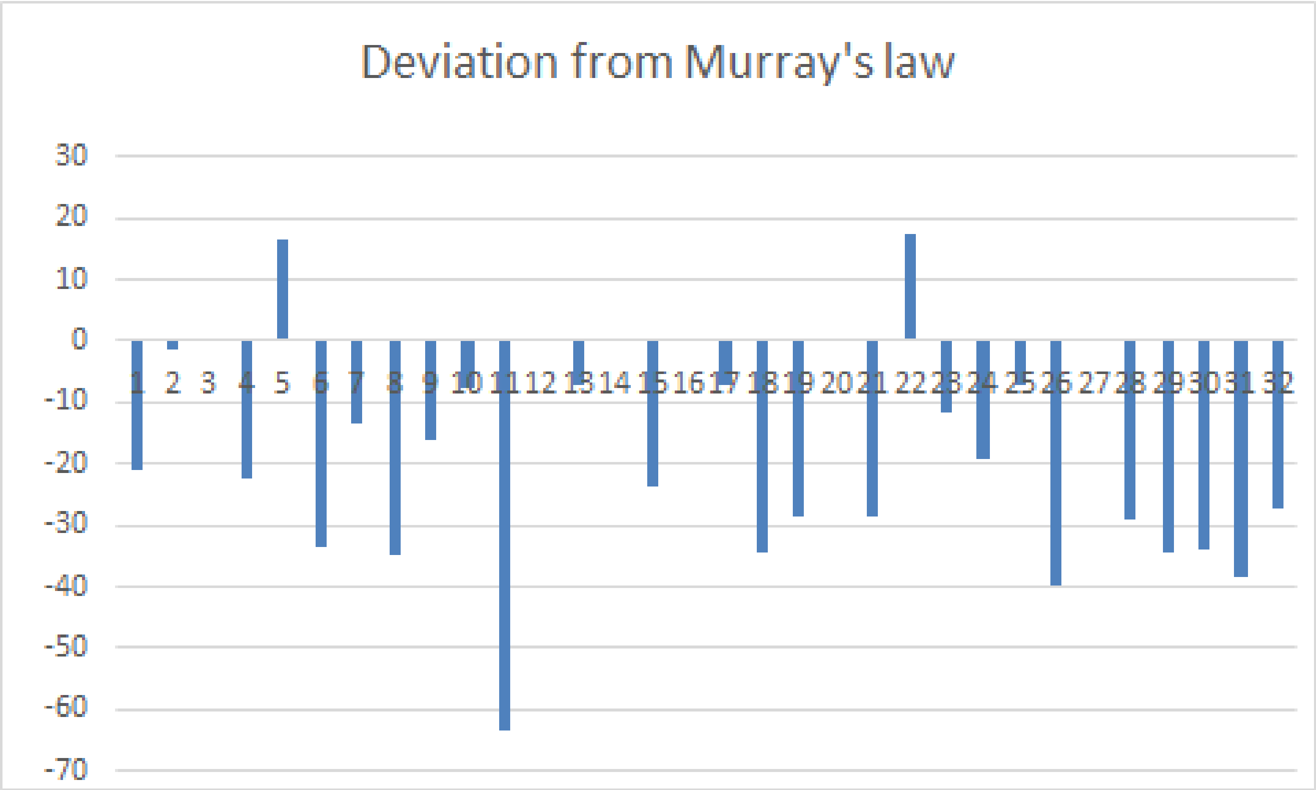

Mean = -21.195 $r_0^{\gamma} = r_1^{\gamma} + r_2^{\gamma}$, $\gamma = 3$

Geometry varieties and mathematical statement

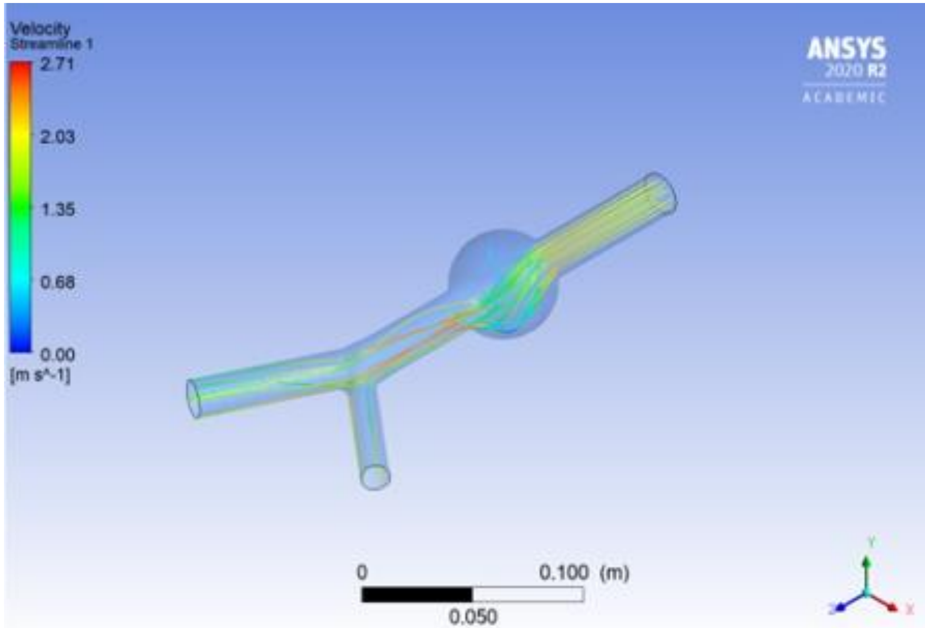

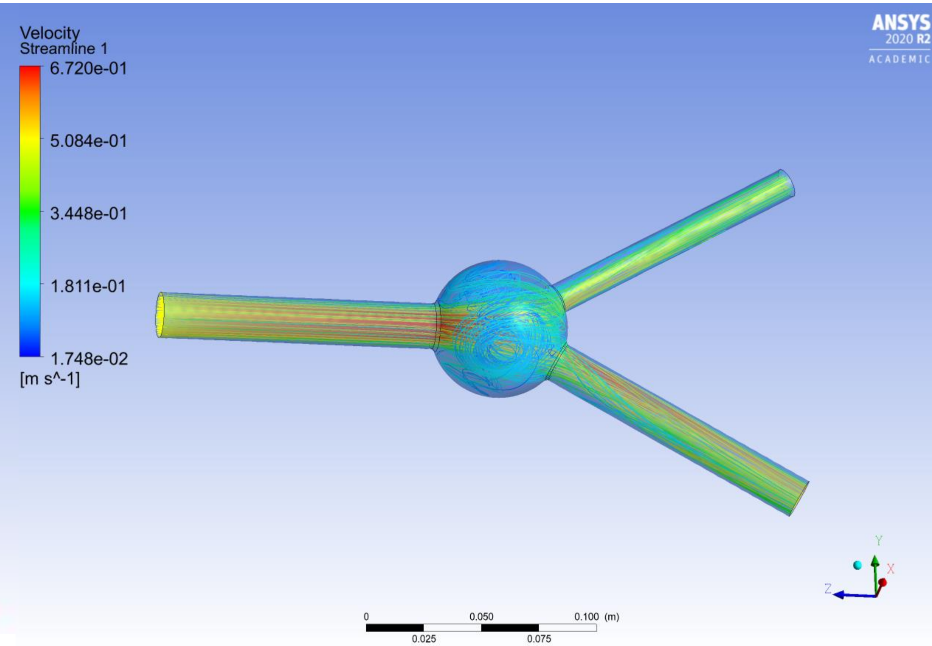

$$
\begin{cases}
\sum_{j=1}^{N} \frac{\partial u_j}{\partial x_j} \equiv \operatorname{div}(\mathbf{u}) = 0, \\
\frac{\partial u_i}{\partial t} + \sum_{j=1}^{N} \frac{\partial (u_i u_j)}{\partial x_j} + \frac{\partial \hat{p}}{\partial x_i} = \sum_{j=1}^{N} \frac{\partial}{\partial x_j} \mu \left(\frac{\partial u_i}{\partial x_j} + \frac{\partial u_j}{\partial x_i} \right),
\end{cases}
$$

No slip wall

Q=0.000154232 m^3/s

Pressure break set at the outlet

Configuring idealized aortha under Murray's law conditions

$$\cos\theta_i = \frac{r_0^4 + r_i^4 - (r_0^3 - r_i^3)^{\frac{4}{3}}}{2r_0^2 r_i^2}, \qquad i = 1,2$$

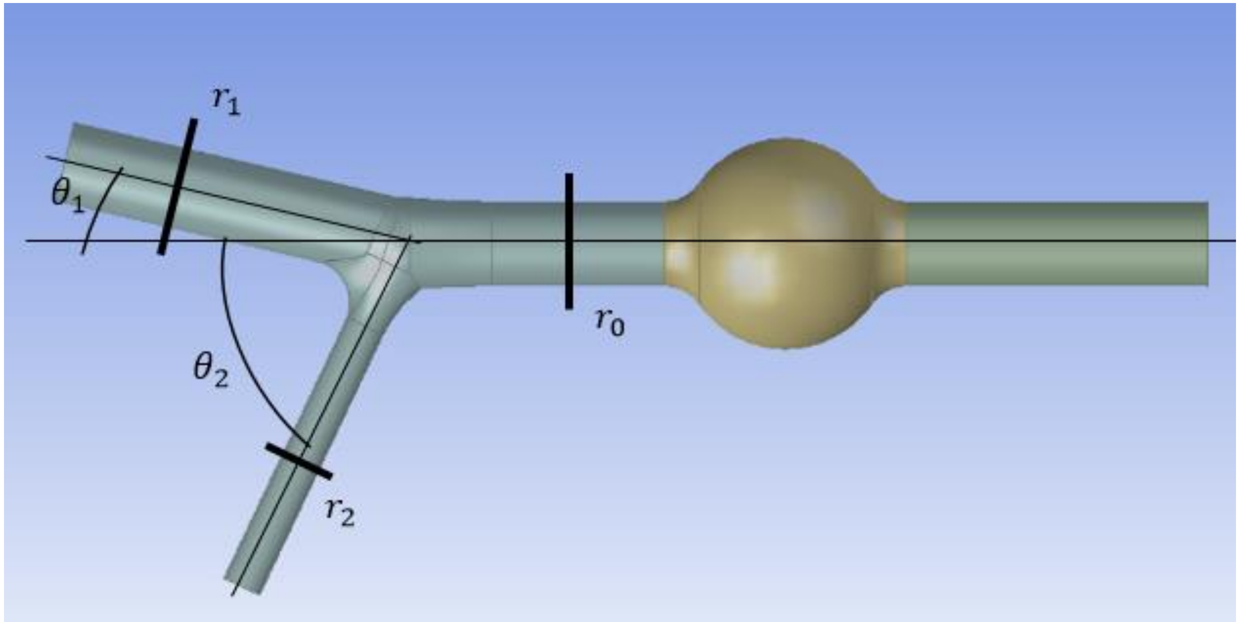

Idealized configuration with AAA, an angle calculated according to Murray’s law and sense of minimizing of the energy of the system

	r2=r1	r2=0.5r1	r2=0.75r1
r0	1	1	1
r1	0,8	0,96	0,89
r2	0,8	0,48	0,67
	37	13	25,5
θ_1	37	64,6	50

θ_2

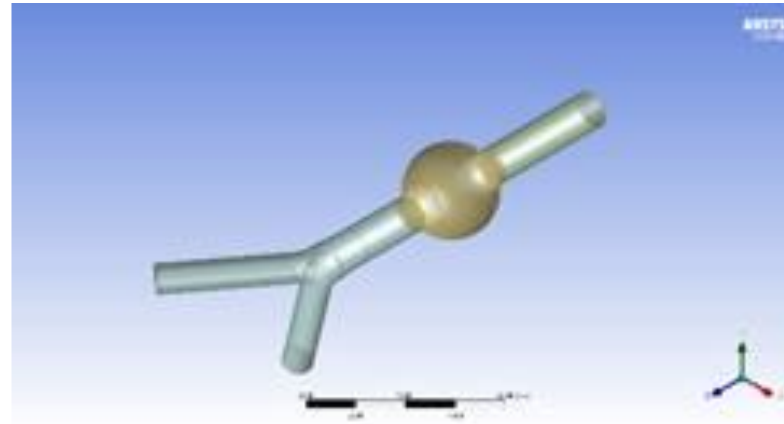

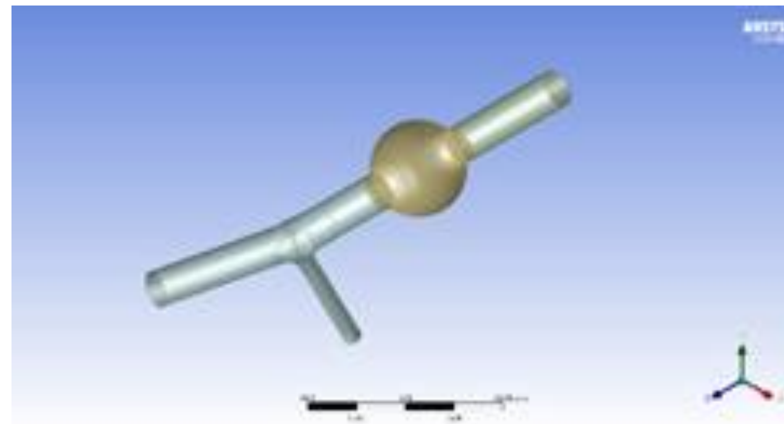

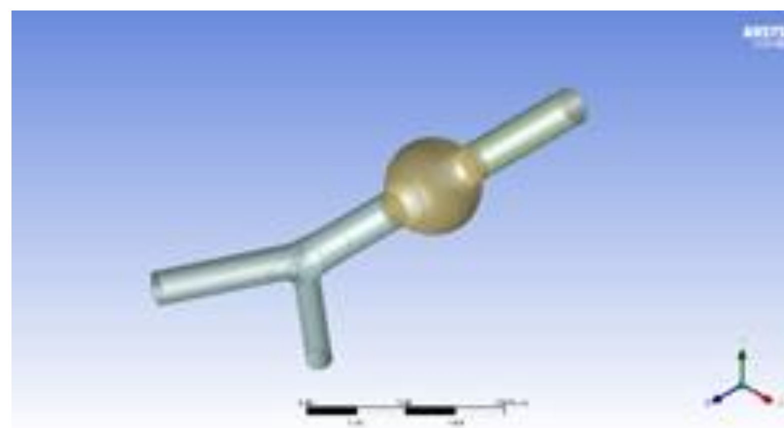

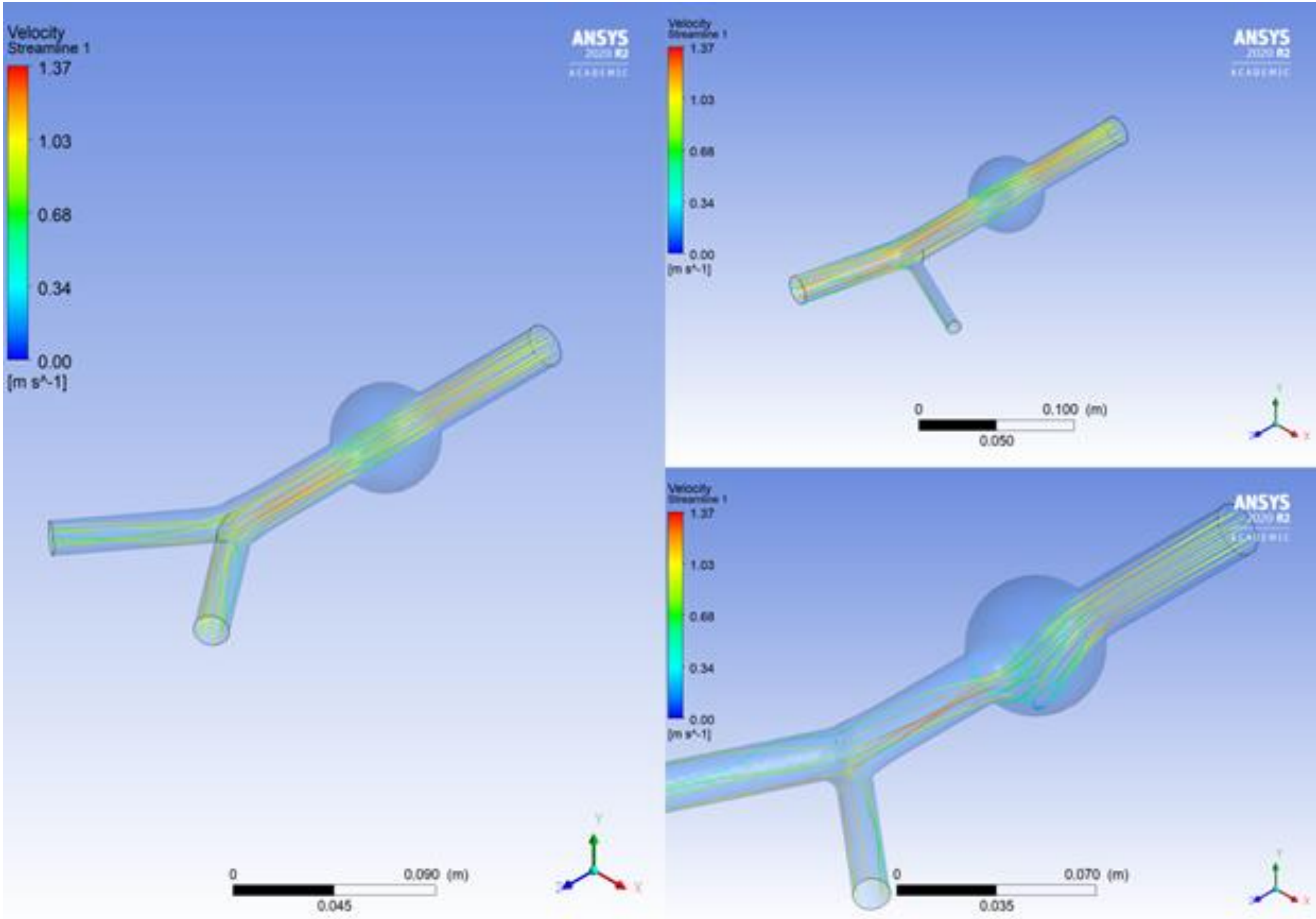

Velocity
Streamline 1
1.37
1.03
0.68
0.34
0.00
[m s^-1]
ANSYS
2020 R2
ACADEMIC
0
0.090 (m)
0.045
0
0.100 (m)
0.050
0
0.070 (m)
0.035

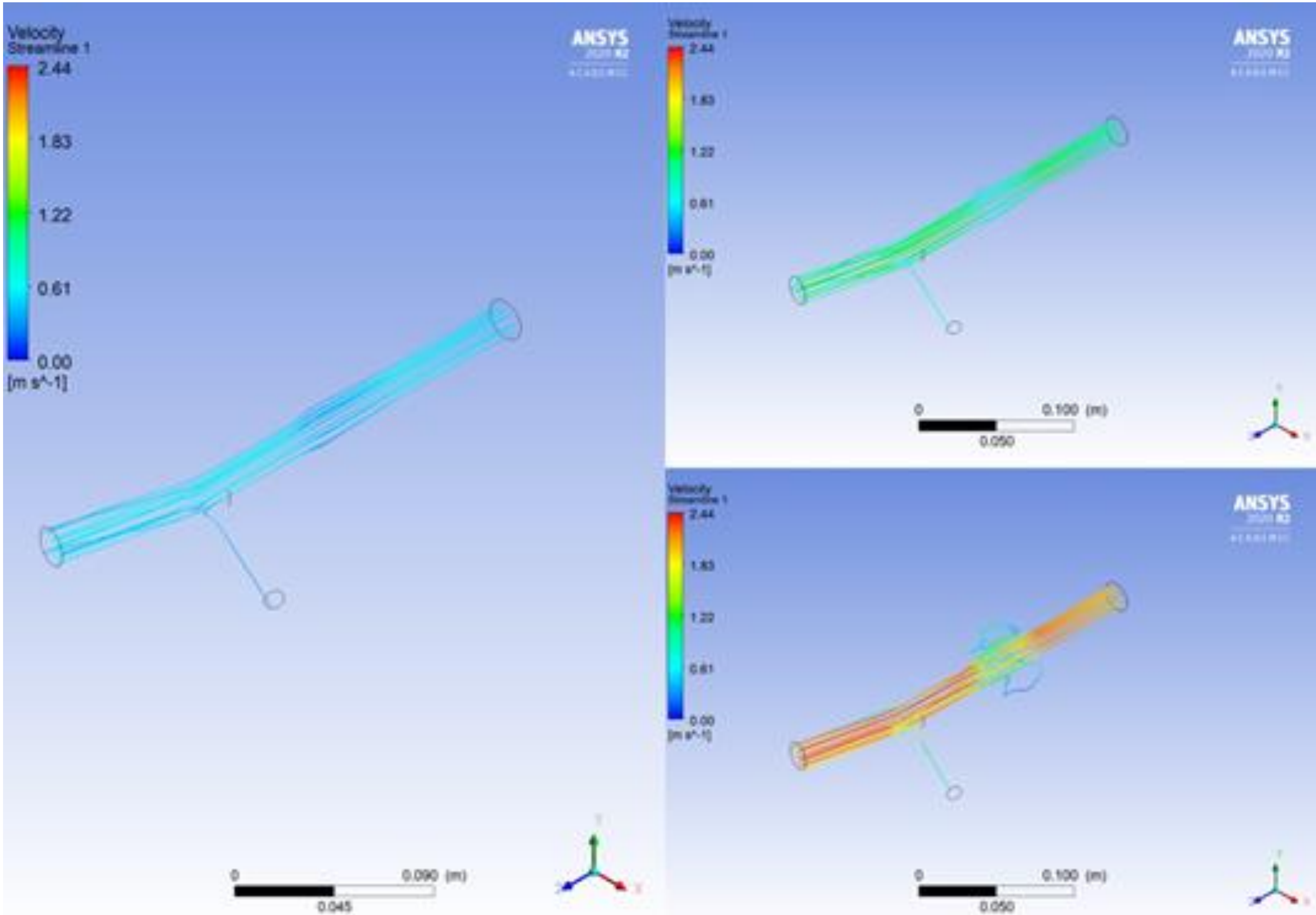
Velocity
Streamline 1
2.44
1.83
1.22
0.61
0.00
[m s^-1]
ANSYS
0
0.090 (m)
0.045
0
0.100 (m)
0.050
0
0.100 (m)
0.050

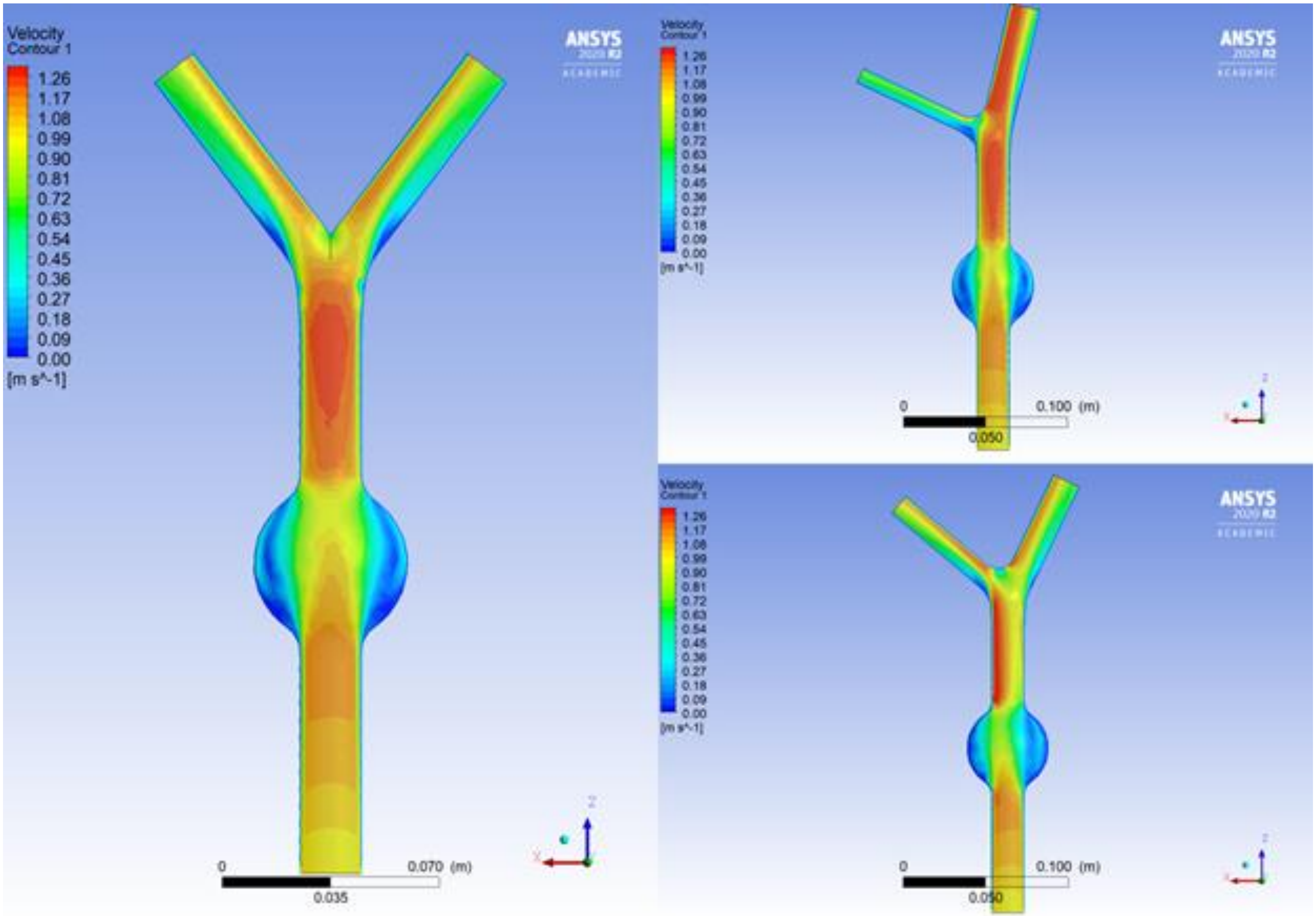
Velocity
Contour 1
1.26
1.17
1.08
0.99
0.90
0.81
0.72
0.63
0.54
0.45
0.36
0.27
0.18
0.09
0.00
[m s^-1]
ANSYS
2020 R2
0
0.070 (m)
0.035
0
0.100 (m)
0.050
0
0.100 (m)
0.050

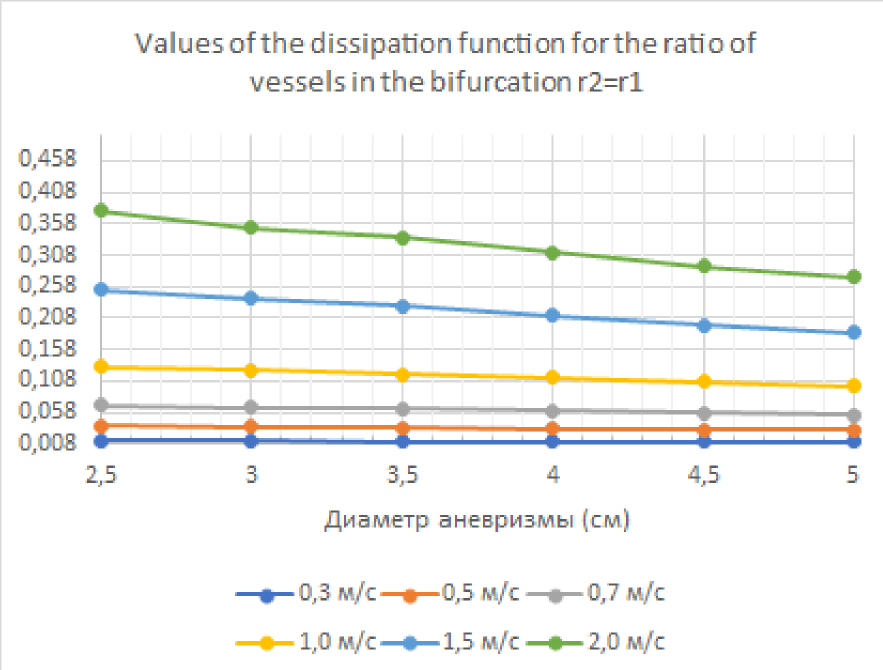

Dissipation function analysis (relative value) with respect to aneurysm size and inflow velocities

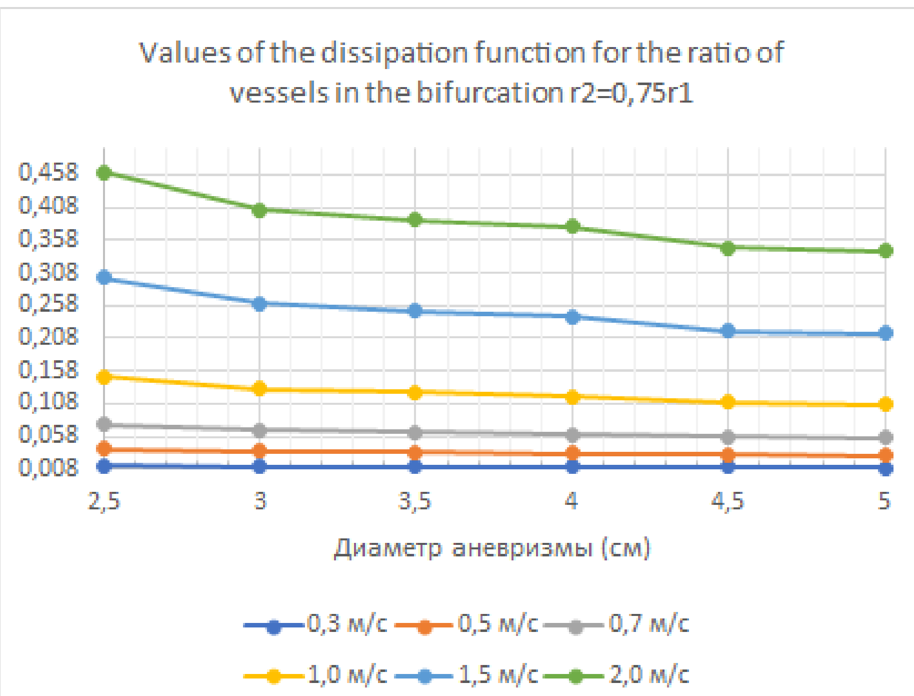

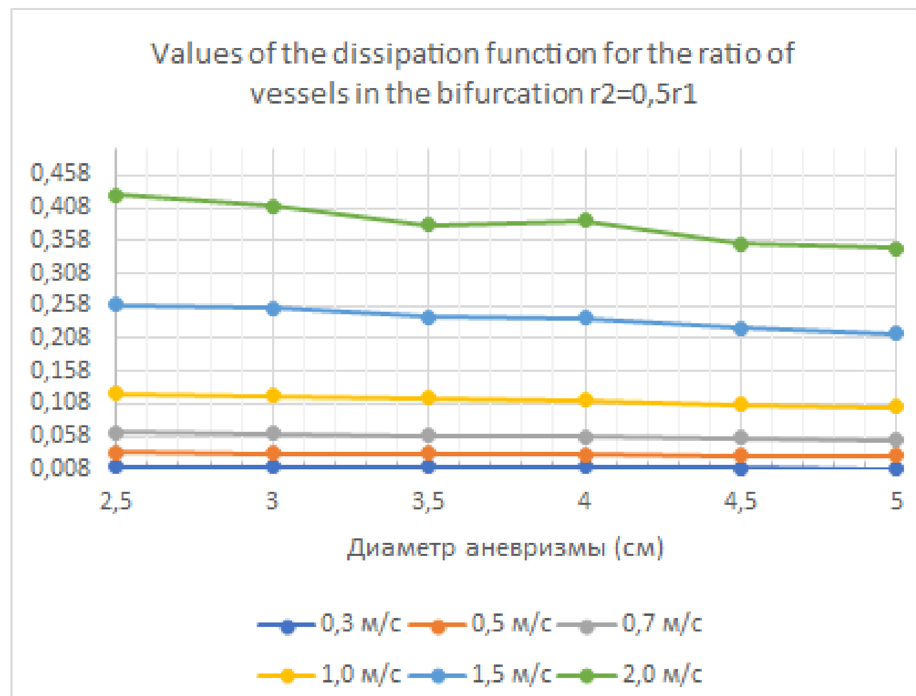

WSS analysis with respect to aneurysm size

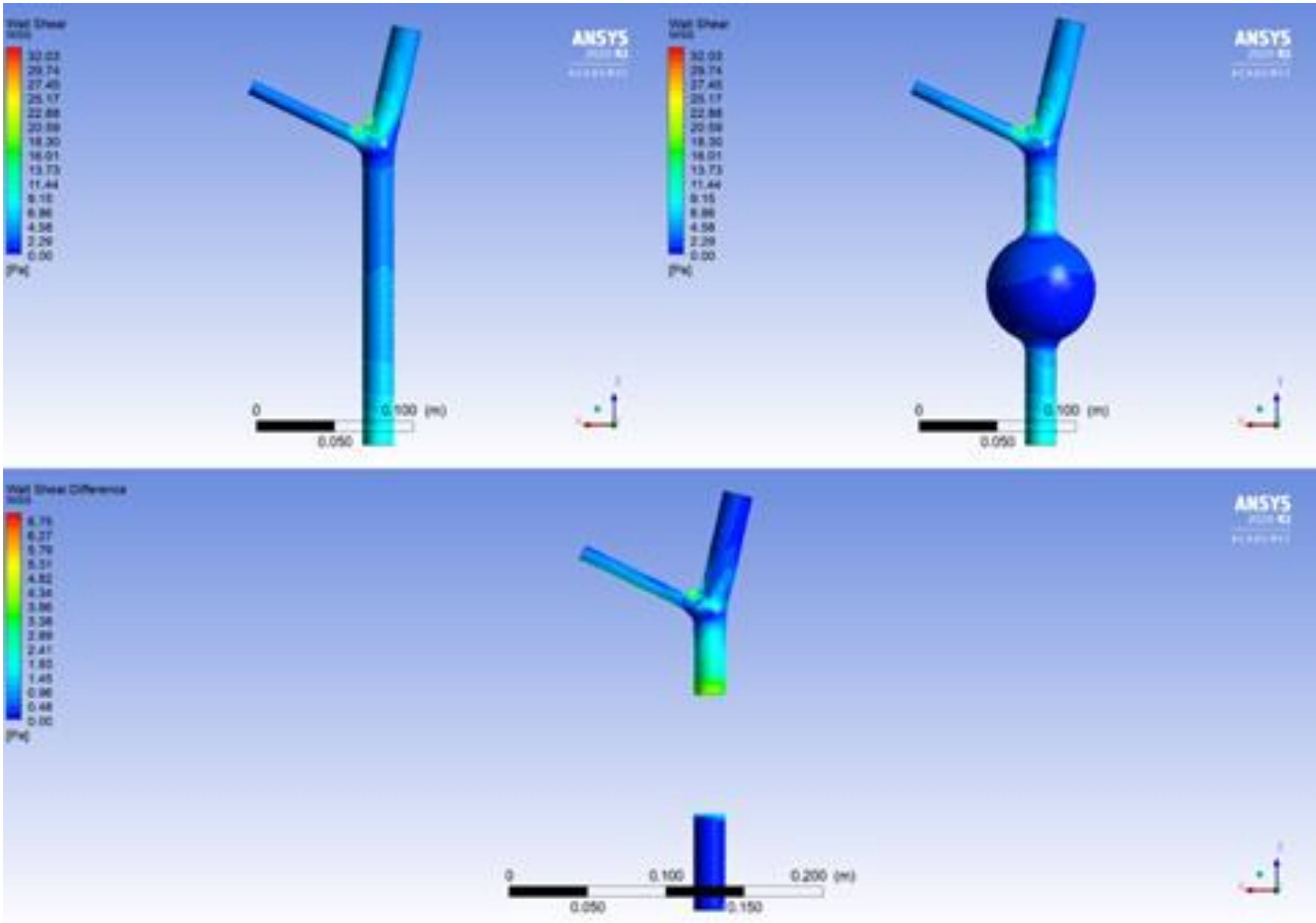

Velocity distribution for the different values of iliac radius ratio (the same angle)

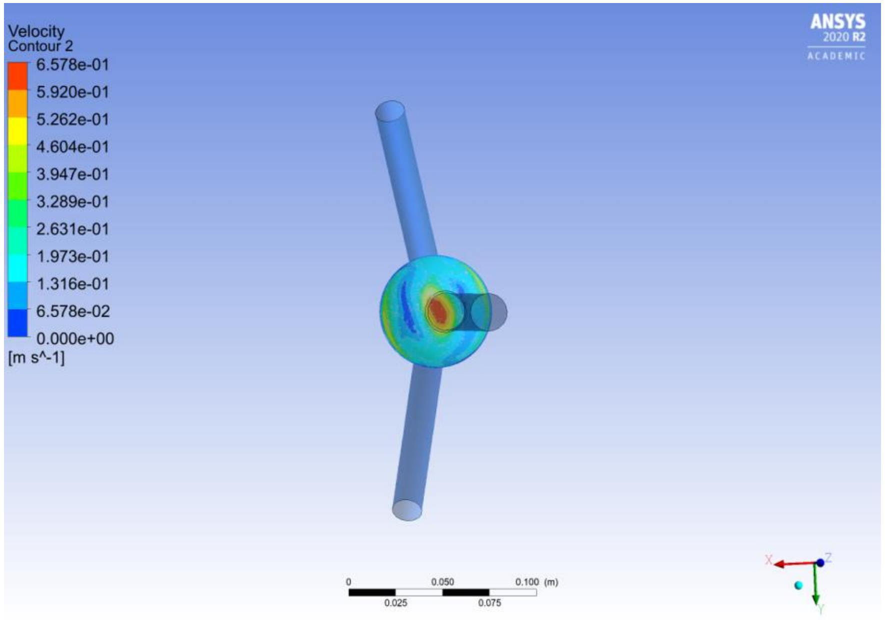

r1=r2

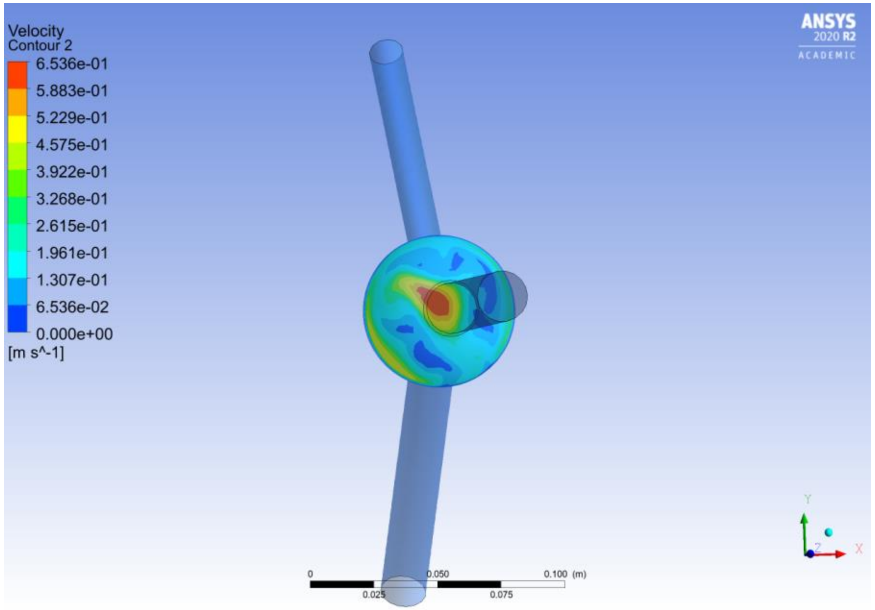

r1=0.75r2

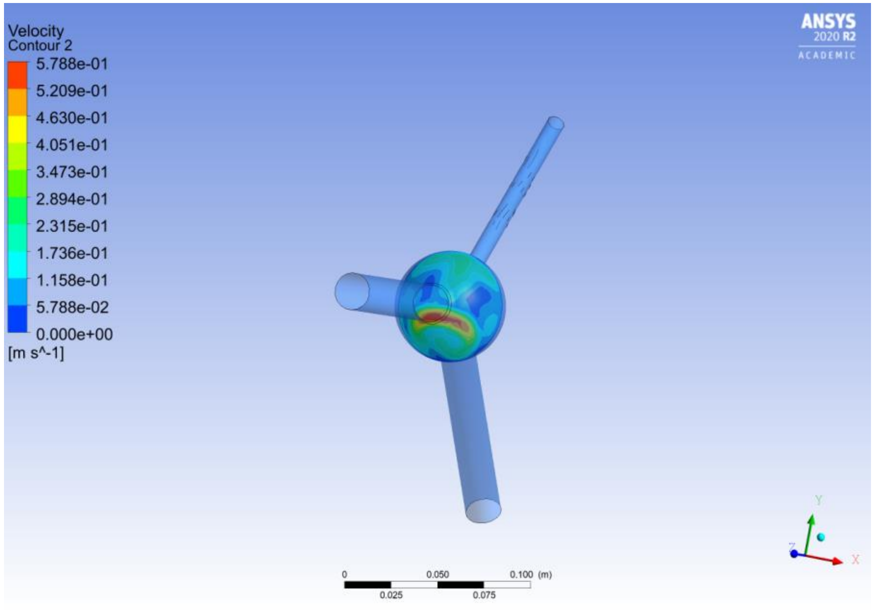

r1=0.5r2

Velocity distribution for the different values of iliac radius ratio (the same angle)

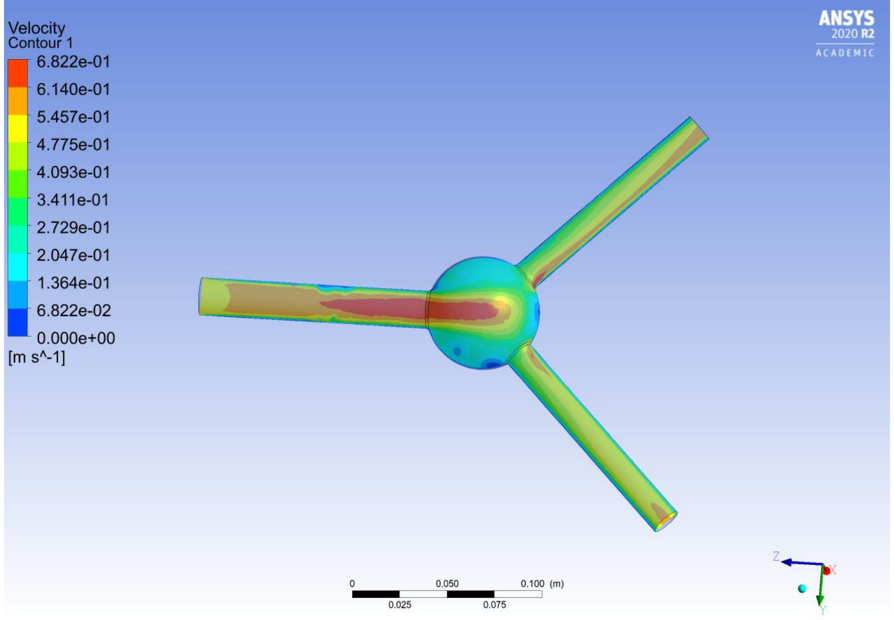

r1=r2

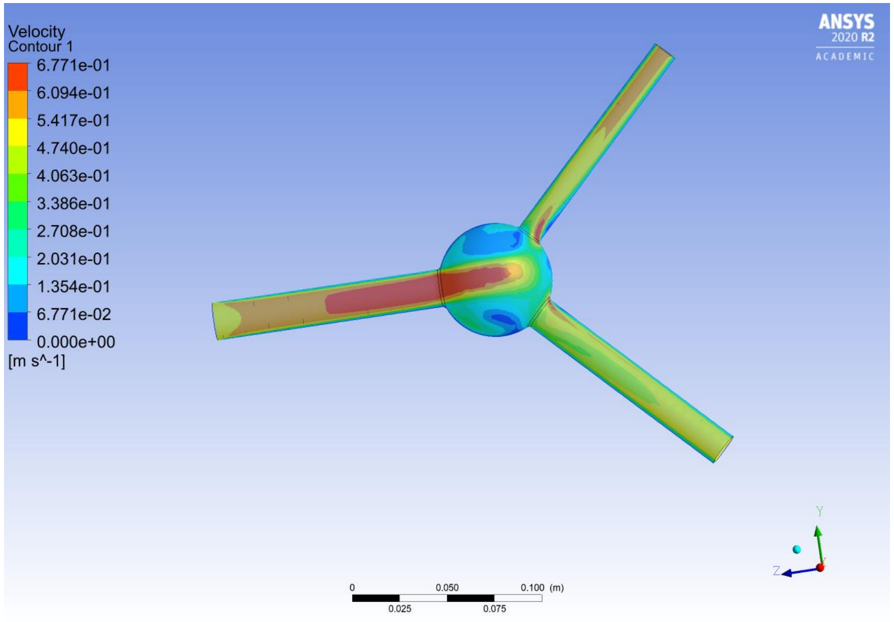

r1=0.75r2

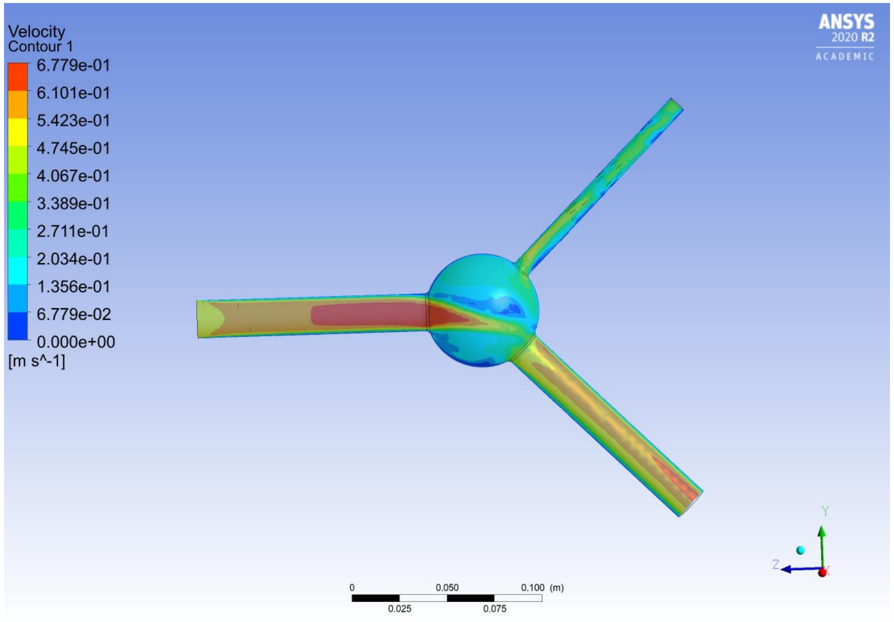

r1=0.5r2

Dissipation function analysis (absolute value) with respect to angle between iliac arteries and their radius ratio

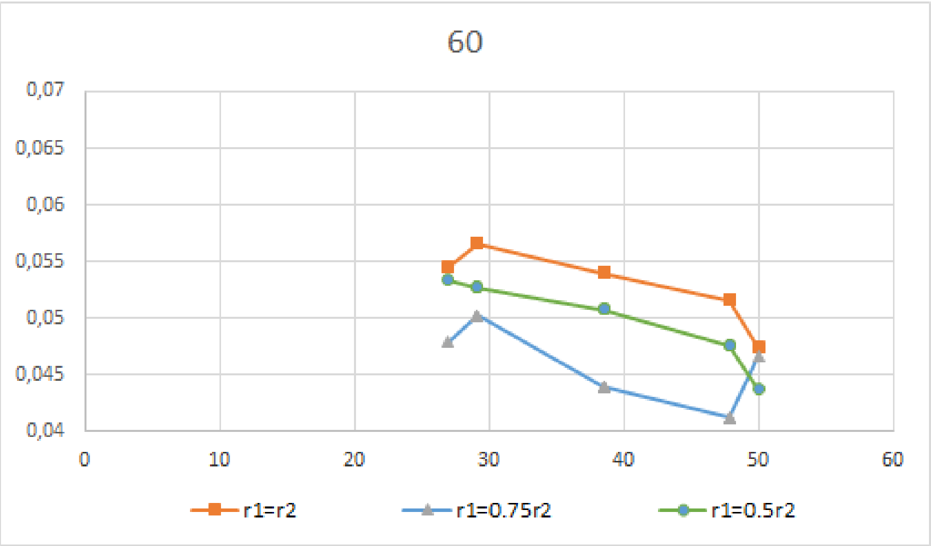

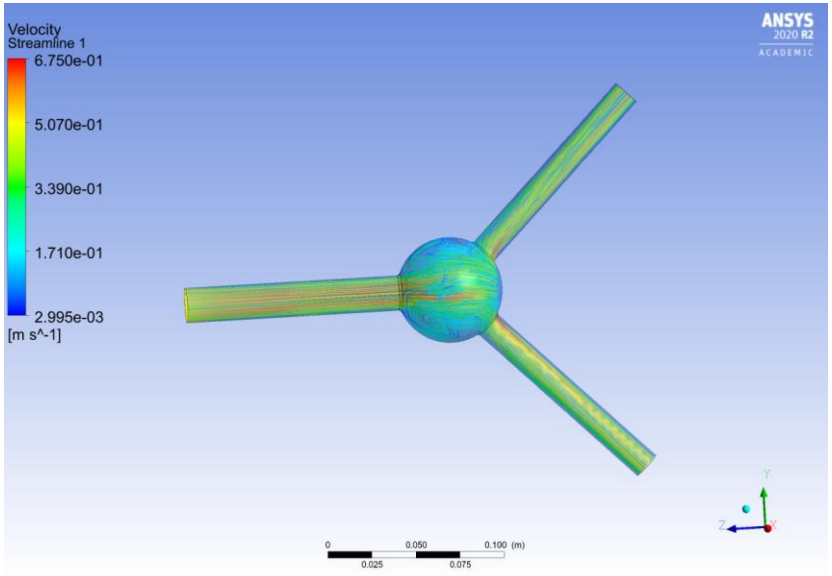

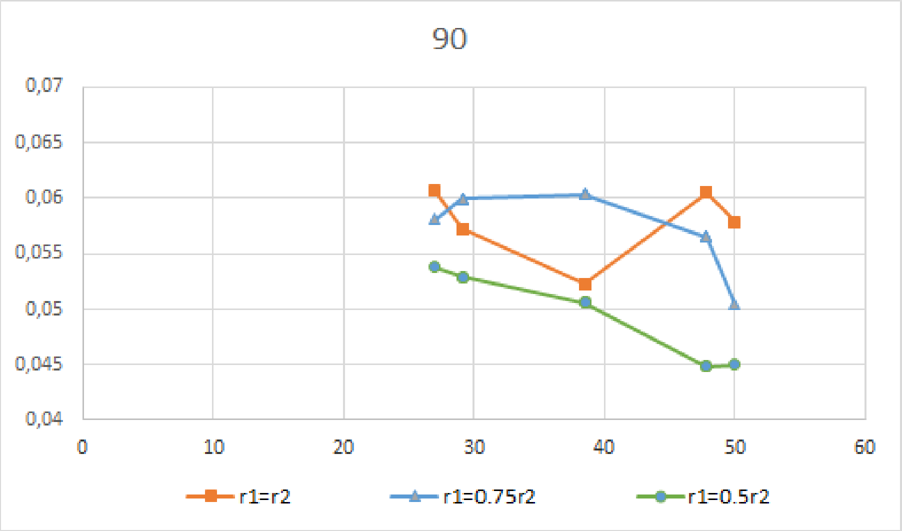

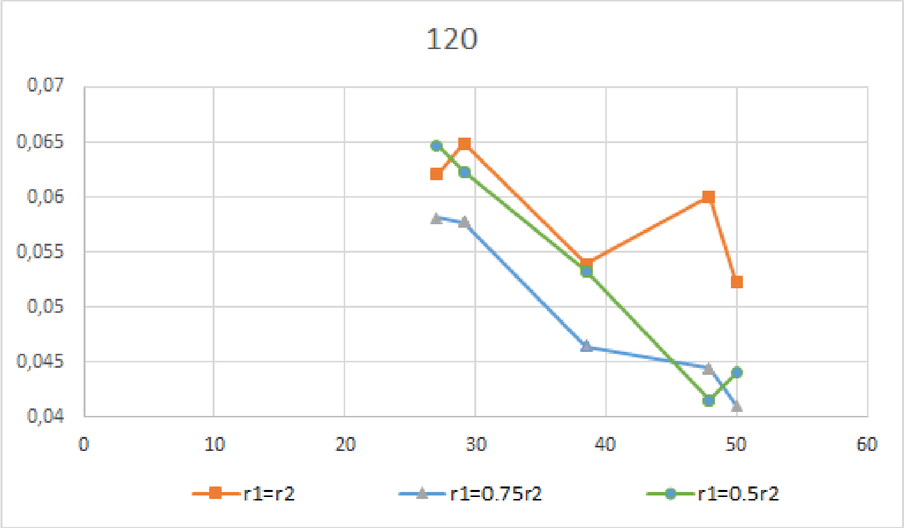

Dissipation function analysis (relative value) with respect to angle between iliac arteries and their radius ratio

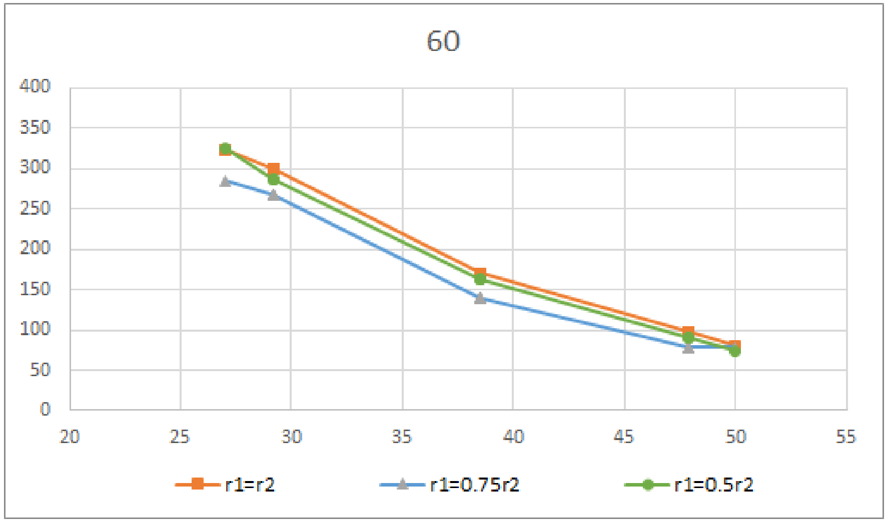

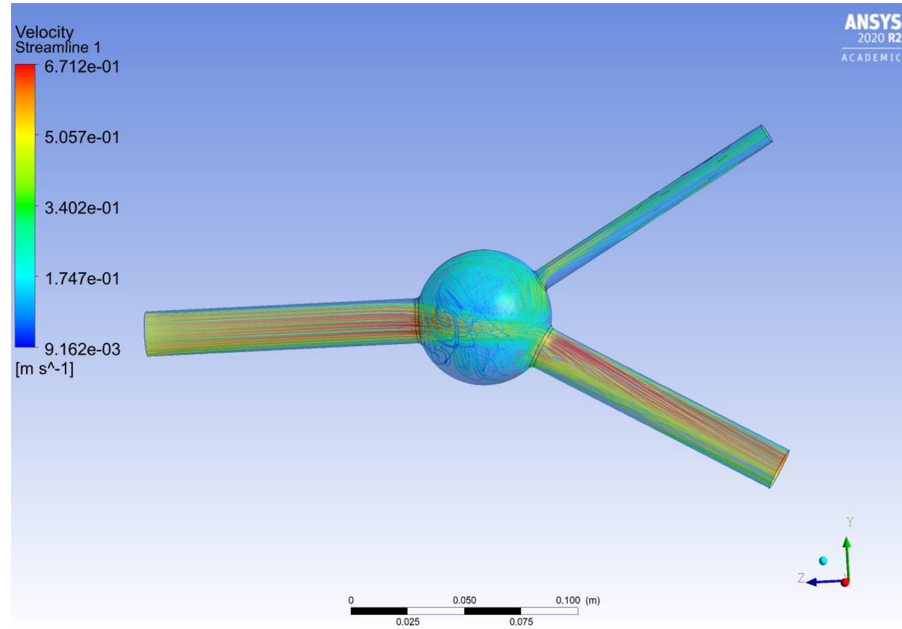

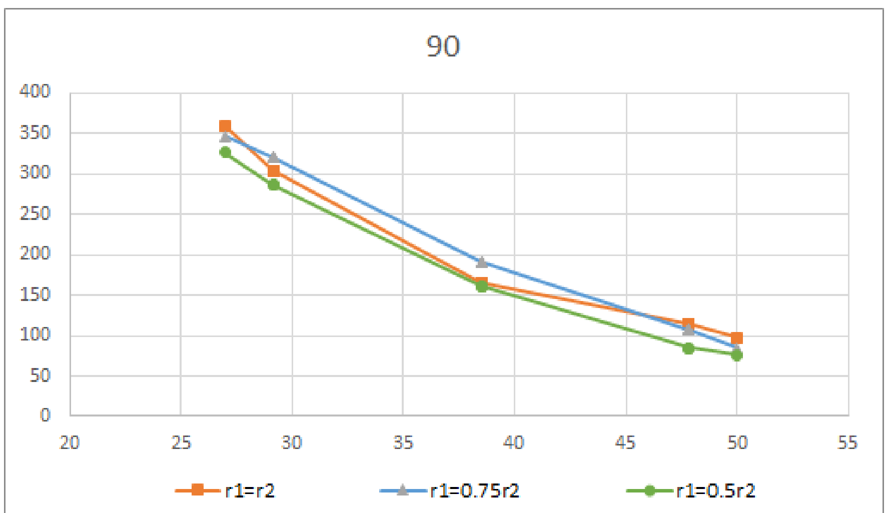

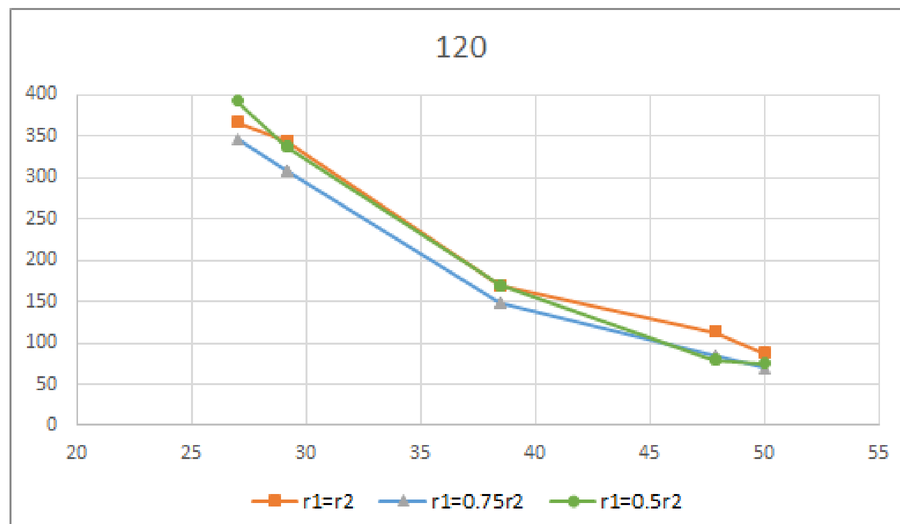

The ZOO of THE PROBLEMS!!!

- Optimal bypass angle and the Shape of an 'arteriometric window'

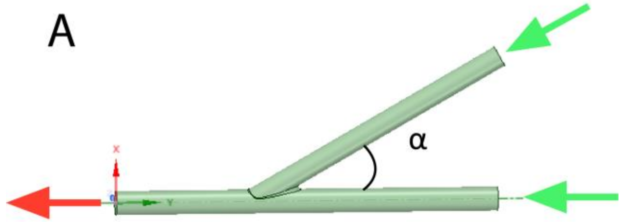

- ARTERIAL vs VIENUS graft

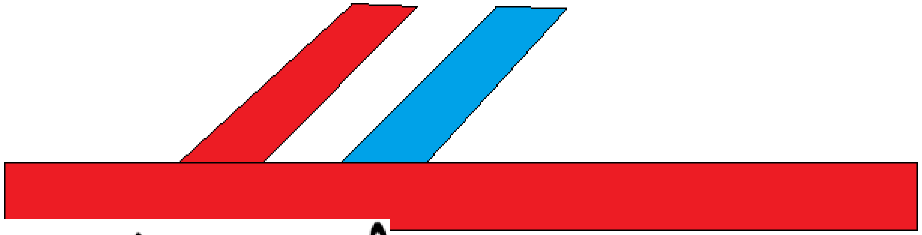

- The necessity of bypass surgery

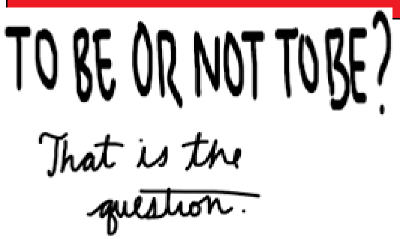

W. Shakespire

- Optimal placement of bypass graft

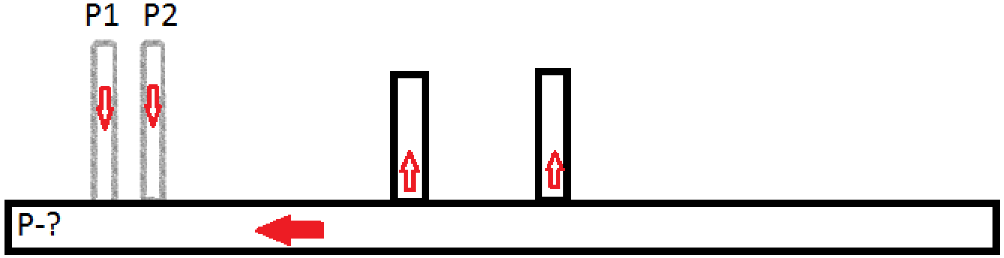

Optimal bypass angle

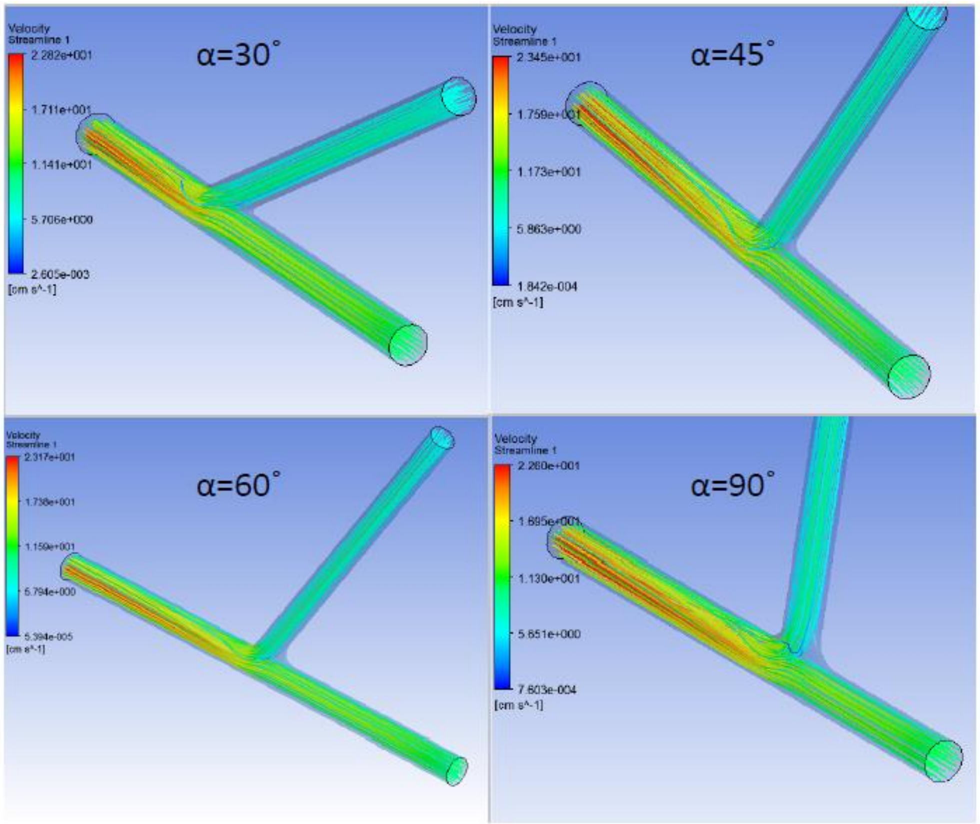

What is going on?

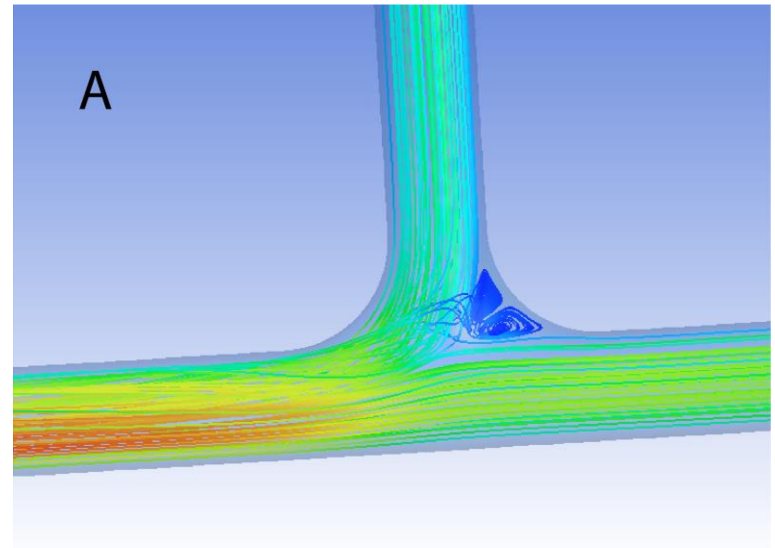

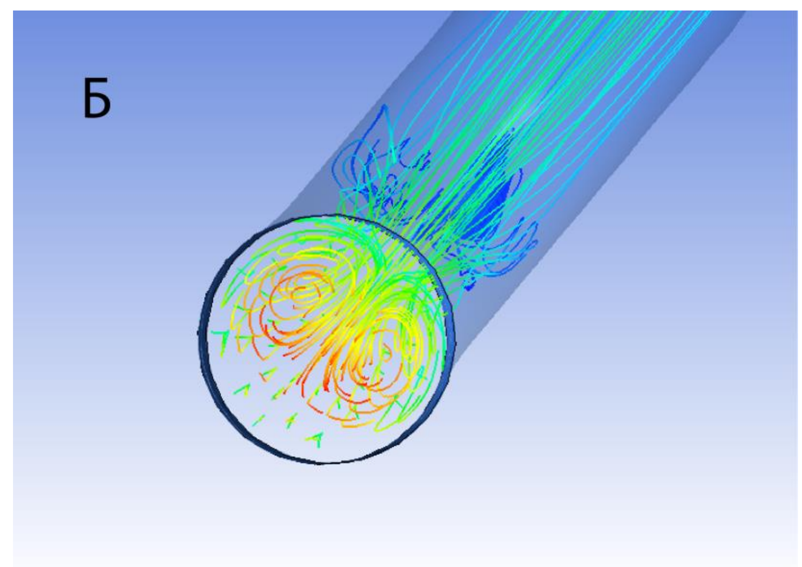

Let's calculate

$$D = 4\mu \int_{\Omega} |\omega|^2 \, d\Omega,$$

Hemodynamic problem

- Steady blood flow for viscous inviscid fluid, Navier-Stokes equations:
- $\begin{cases} \rho(u\nabla u - \mu\Delta u) = -\nabla p \\ div\, u = 0 \end{cases}$
- u – velocity
- ρ – density
- p – pressure

For the simulations we used unstructured tetrahedral mesh with 5 inflation layers.

Value of the power of dissipation integral with respect to the parameters

Ratio of diameters

Ratio of the velocities

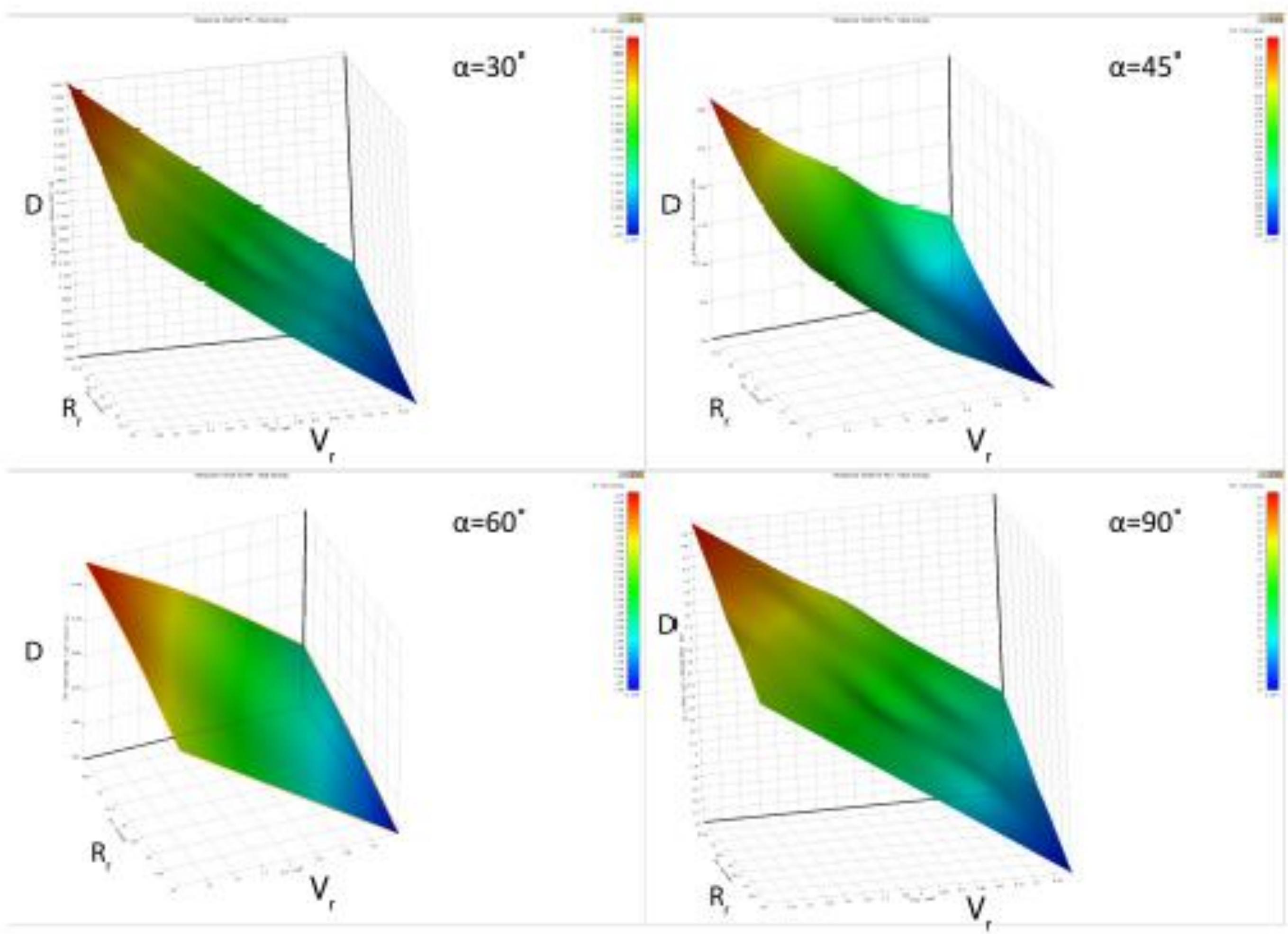

Optimal bypass placement angle analysis

Wall shear stress values (Max), Pa

$\pi/6$	$\pi/4$	$\pi/3$	$\pi/2$
0,828	0,421	0,468	0,527

V(cm/s),R(mm)	π/6	π/4	π/3	π/2
Minimal values of D integral, J/s $*10^{-7}$				
V_1=6, R_1=14	**13523**	17192	**13365**	**13892**
V_1=6 ,R_1=13.896	14799	**16387**	16246	15736
Maximal values of D integral, J/s $*10^{-7}$				
V_1=14 ,R_1=10,1	**36734**	**48062**	**42211**	**39886**

2. The mechanics of arterial tissues

Cerebral aneurysm mechanics

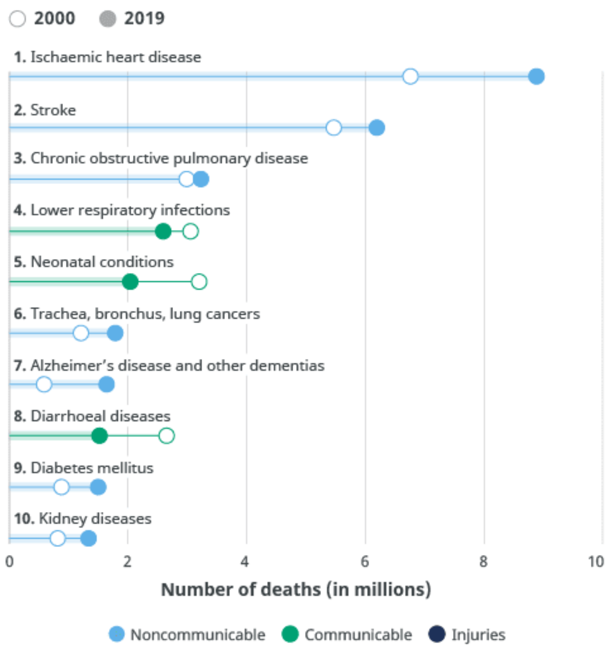

© WHO

According to W.H.O. aneurysm associated diseases are among the most common causes of death in the world.

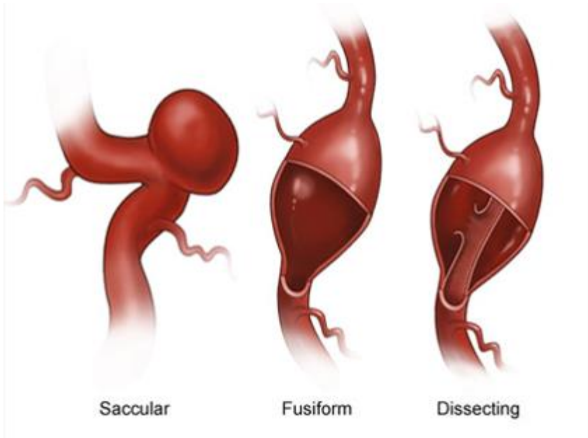

© Mayo Clinic

Types of aneurysm:

- Saccular,
- Fusiform,
- Dissecting;

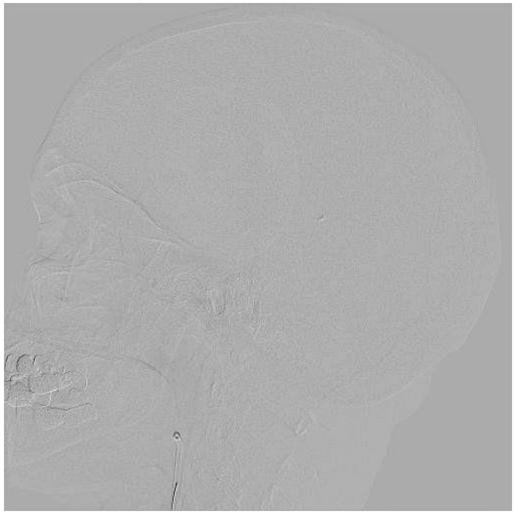

Risks

Is surgery necessary?

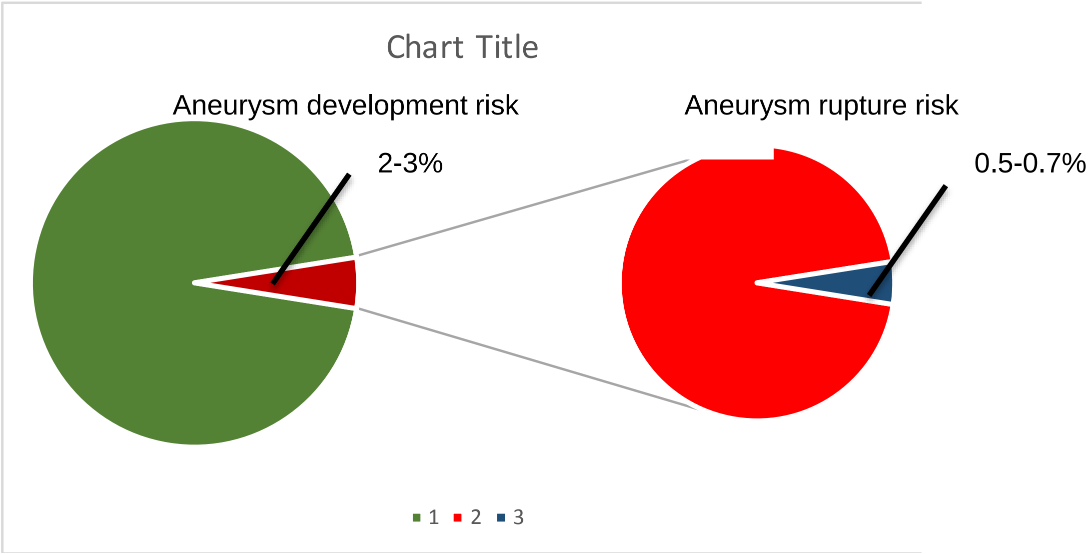

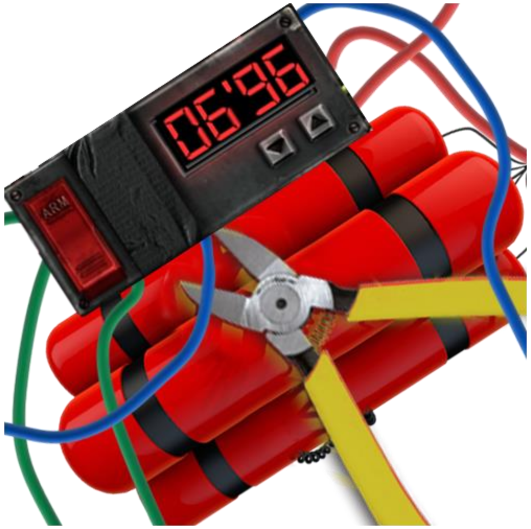

Risk of rupture ~

Risk of developing postoperative complications (0.6%)!!!

Which one should be cutted?

ISUIAI, *Lancet* 2003; 362: 103–10

The history of mechanical test

- The first mechanical test with an intracranial aneurysm wall performed by **Scott 1971**,
- Nowadays the leading position has **PITT** with **A. Robertson** as a head of the research, and **V. Costalat** from **Universitet of Montpelier**;

Special sessions dedicated to cerebral aneurysms held at:

- CMBE 2017
- WCB2018
- VPH2018
- CMBE2019
- ESBiomech2019
- VPH 2020
- ESBiomech2021

A. Robertson, PA, US

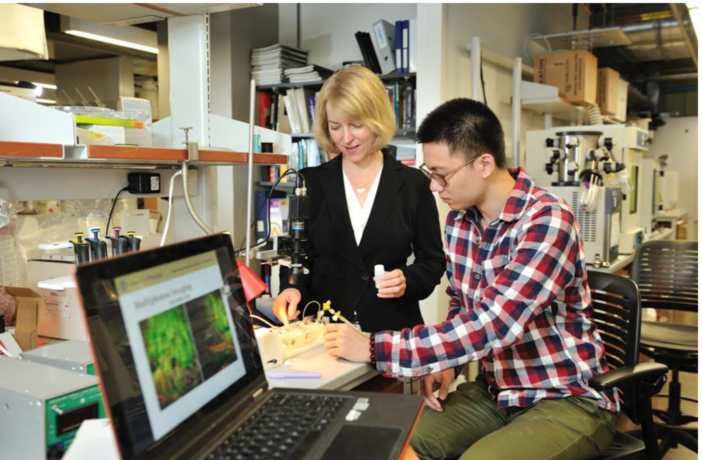

V. Costalat, France

Methods. Mechanical test

Specimen before the start of the experiment.

Specimen in the *Zwick&Roell* rupture machine

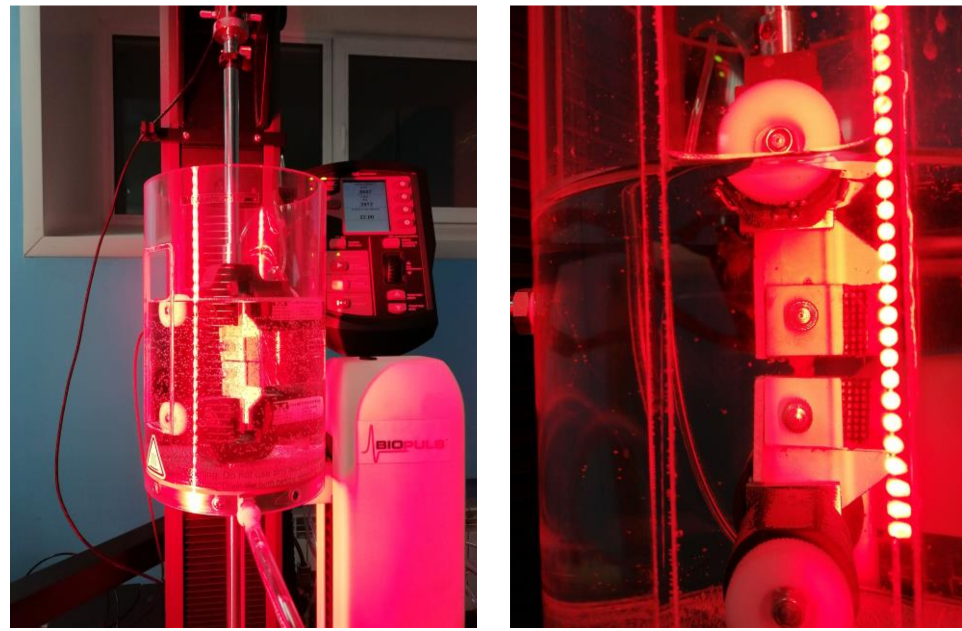

Specimen in the *Instron 5944* rupture machine

Methods. Stages of the loading

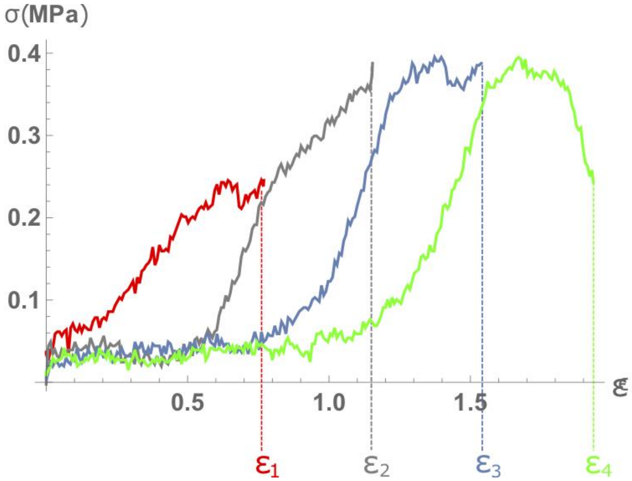

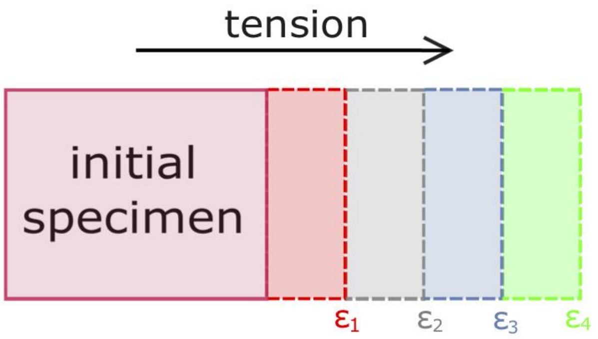

While conducting the experiment we took into account well-known phenomenon for biological tissues – **preconditioning**. The need to consider this phenomenon was due to the significant role of the matrix in the mechanics of such tissue. Taking into account its relaxation during the experiments ensures that the true stresses in the sample are correctly accounted for. This technique was used for the initial stages (stage 1-5 depending on the sample), and in the next stages the effect of this condition was not noticed.

Sommer, G., Regitnig, P., & Holzapfel, G. (2006). *Biomechanics of human carotid arteries: experimental testing and material modeling*. 5th World Congress of Biomechanics, München, Germany

Hierarchy of the models

Ultimate strain, that admit no more than 20% deviation from the model

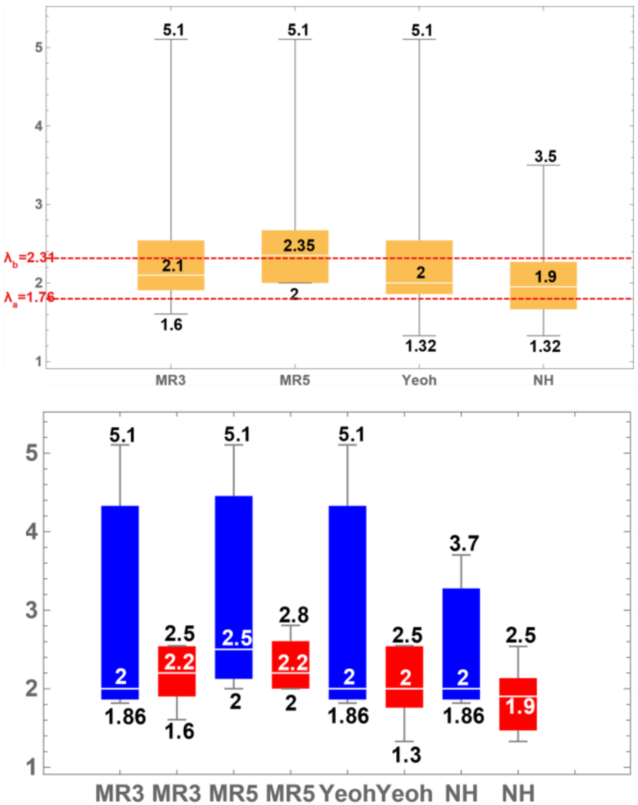

Different types of approximation

Yellow – all samples
Blue – unruptured aneurysms
Red – ruptured aneurysms

MR3 – 3-parameter Mooney-Rivlin model

MR5 – 5-parameter Mooney-Rivlin model

YEOH – Yeoh model;

λ_a – elastin and collagen bear loading

λ_b – elastin ruptures, only collagen bears loading

Parshin et al. On the optimal choice of a hyperelastic model of ruptured and unruptured cerebral aneurysm // Scientific reports. 2019

Fluorescence

The 210-350 nm laser is used with the size of spot approximately 5x14 мм. Fluorescence spectra of resected vessels' fragments were measured. During the spectrometer's exposure time (1 sec.) the emitting pulses were accumulated. The linearity of fluorescence was monitored. Pulse energy did not exceed 200 mkJ per pulse. The measurements in laser wavelength diapason 210-290 nm were performed using a special filter (short-wave boundary at 300 nm), in 300-350 nm – using BC-8 filter. Each spectrum was normalized with total energy of laser irradiation during the exposure time and relative spectral sensitivity of the spectrometer.

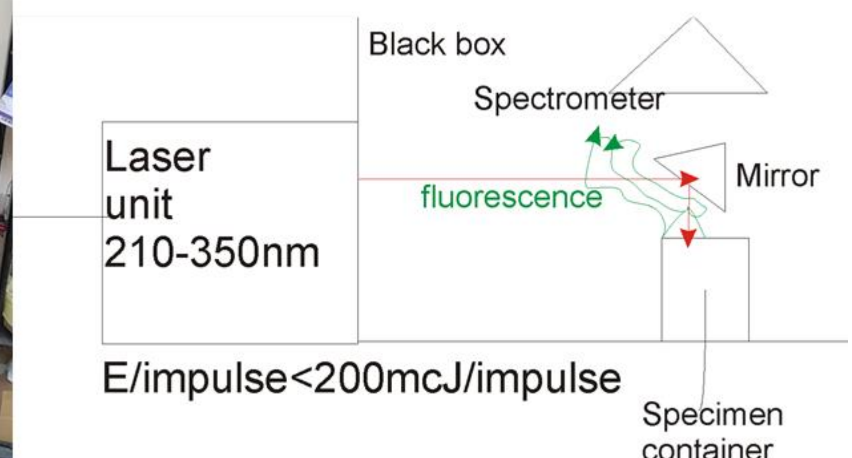

Fluorescence

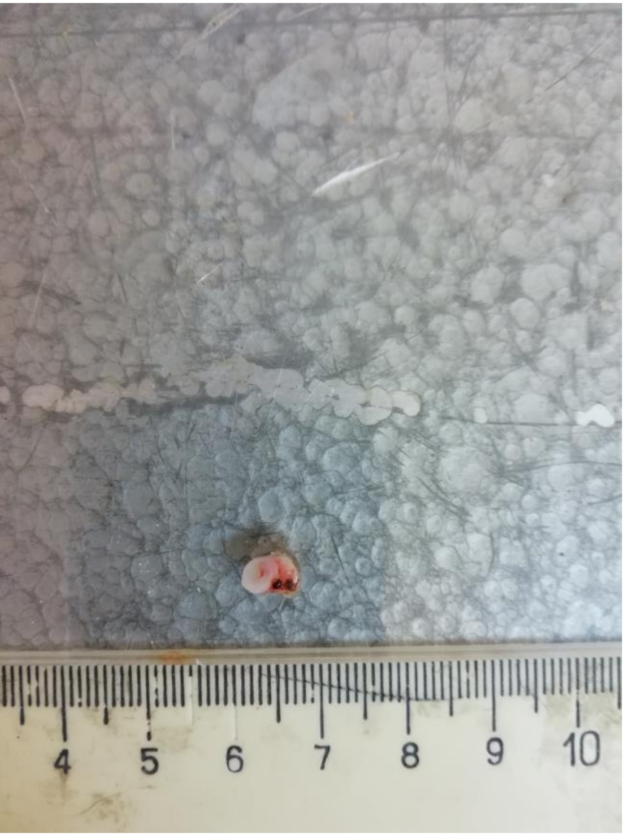

Before the start of the experiment we clean blood pieces from the specimen and prepare a rectangular shape specimen. For each laser wavelength we perform 20 acquisitions.

Fluorescence

Spectra were analyzed with the principal component method. All spectra are well described by the sum of three components, presented in the picture below. As the components are alternating, spectra of real fluorophores are their linear combinations. By selection method we obtained spectra of narrow peaks.

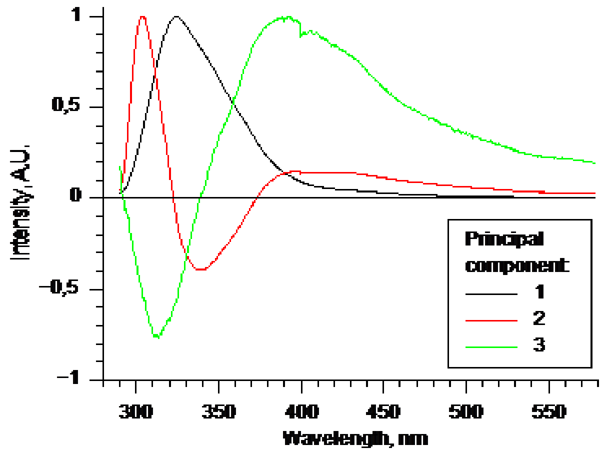

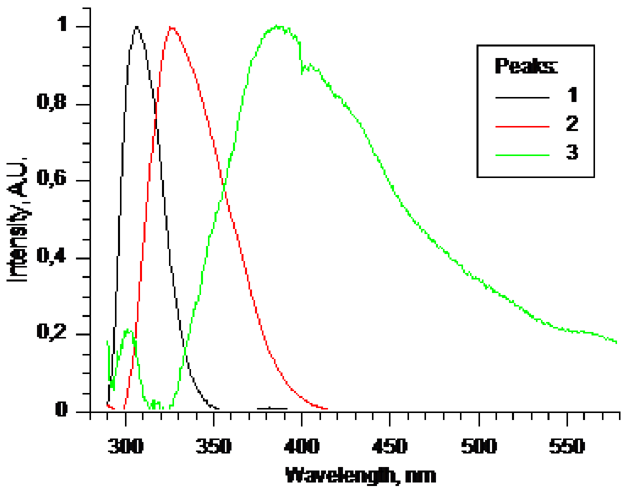

Fluorescence results

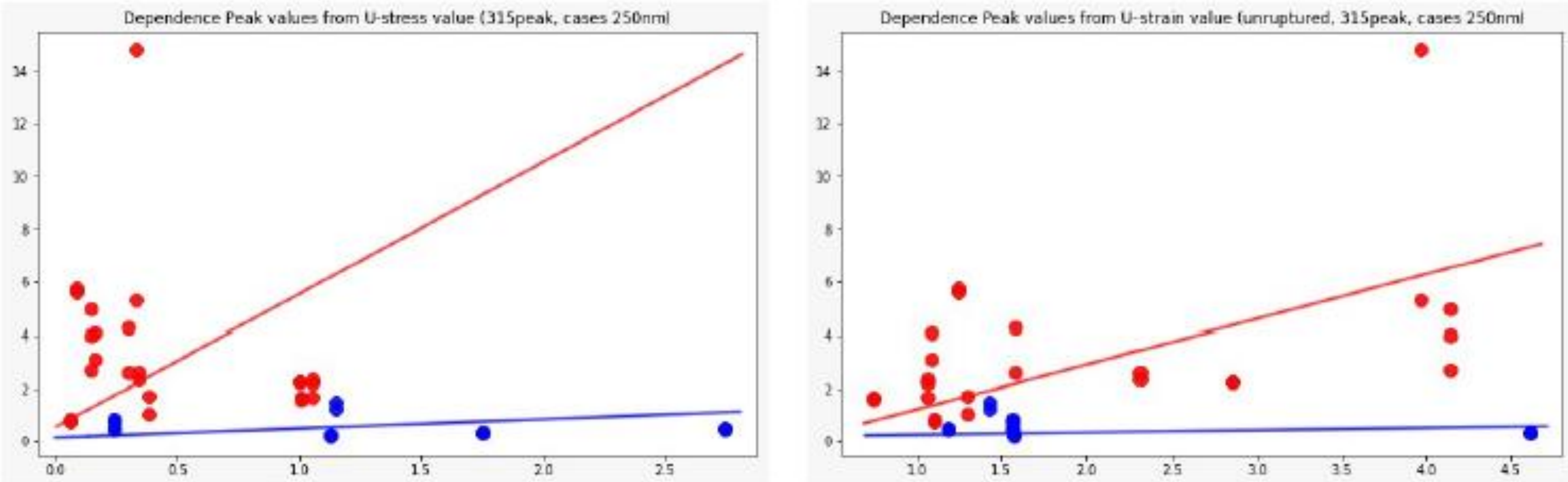

(a) (b)

Red – Ruptured aneurysms
Blue – Unruptured aneurysms

250nm, 315nm peak
A – ultimate stress
B – ultimate strain

Peak Wavelength/ Normalized by	315	370	400	440	500
315	-	0.1869	0.028978	0.0769	0.0002
330	0.34977	0.01175	0.01176	0.026829	0.000119
370	0.18692	-	0.20549	0.05546	0.00119

P-values

E. Tsibulskaya et al. Biomedicines 2021 May 12

Mechanical properties of AAA

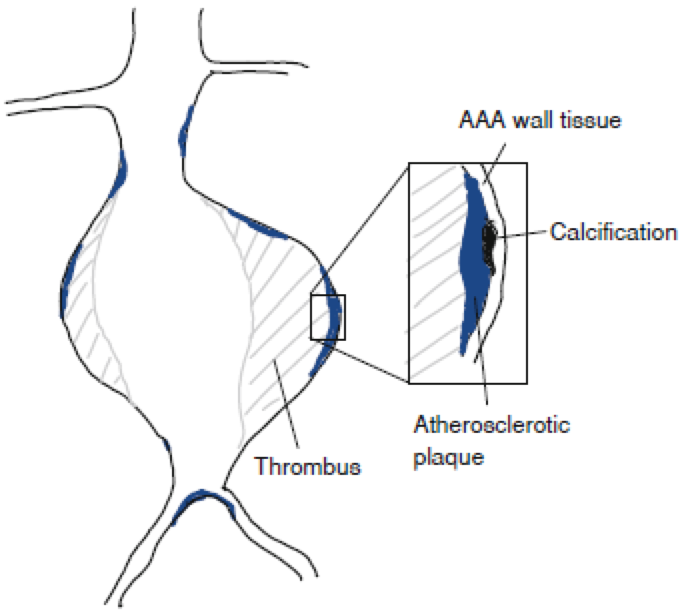

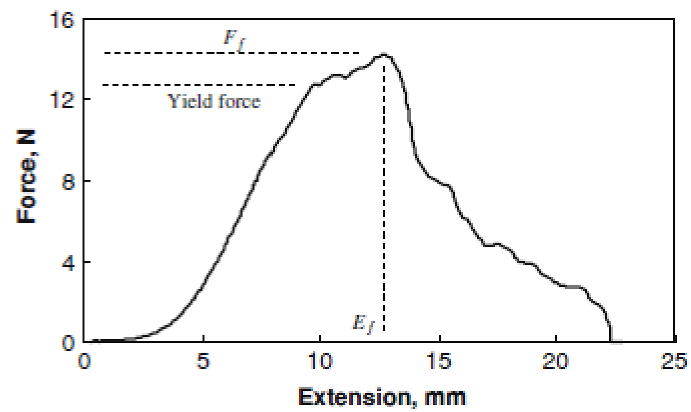

Clinical significance of understanding
by Madhavan L. Raghavan and Erasmo Simão da Silva in
https://link.springer.com/book/10.1007%2F978-3-642-18095-8

Different approaches to study AAA evidence (from experimental to simulations)

Rupture zone predicting

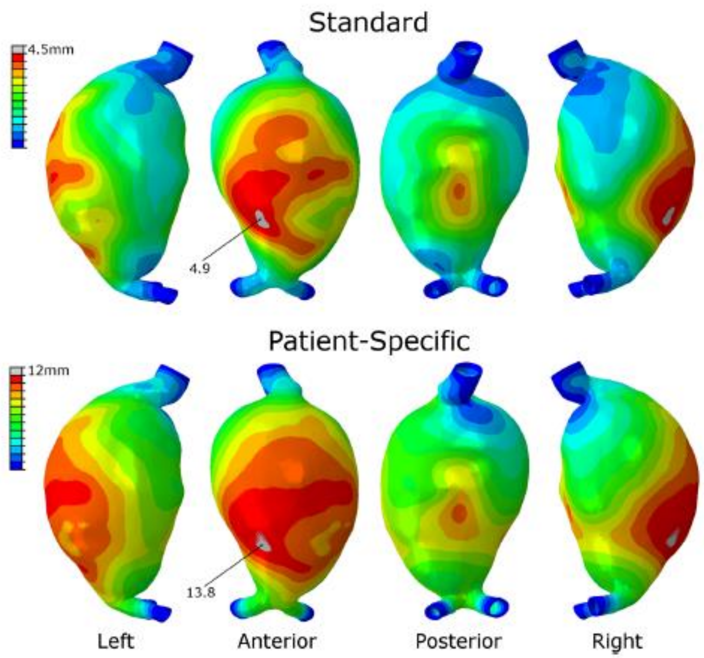

Displacement contour plot (from Doyle et al 10.1002/cnm.2515)

AAA finding (borrowed from Sazonov et al 10.1007/s10237-017-0884-8)

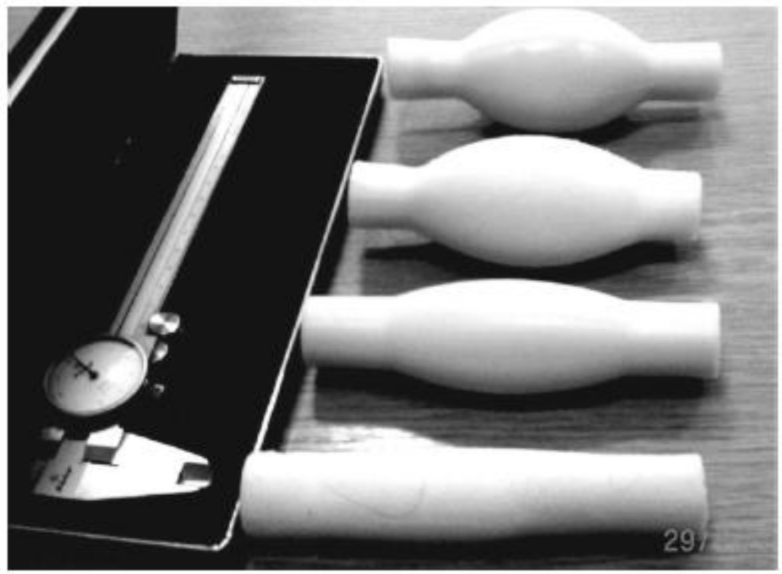

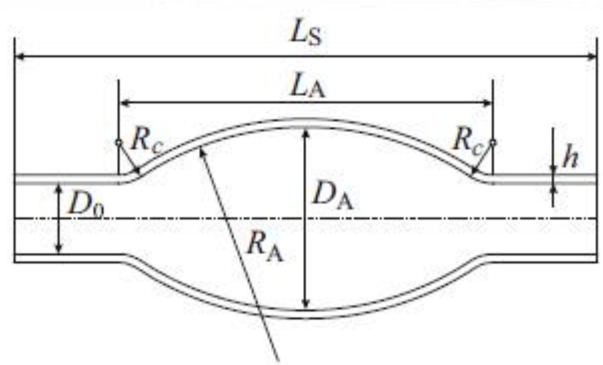

Stages of the mechanical testing (1)

Sample after retrieval and transportation

preparation of sample shape for testing

Stages of the mechanical testing (2)

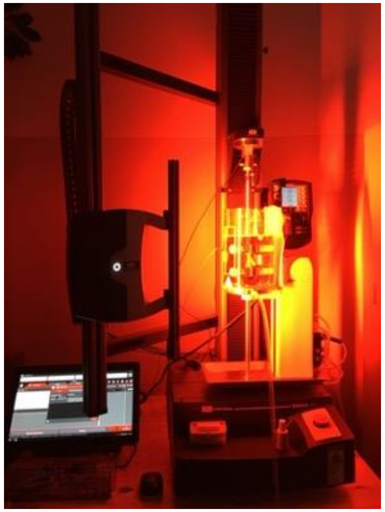

Carrying out a mechanical test in a bio-bath at a temperature of 37C on an Instron 5944 machine

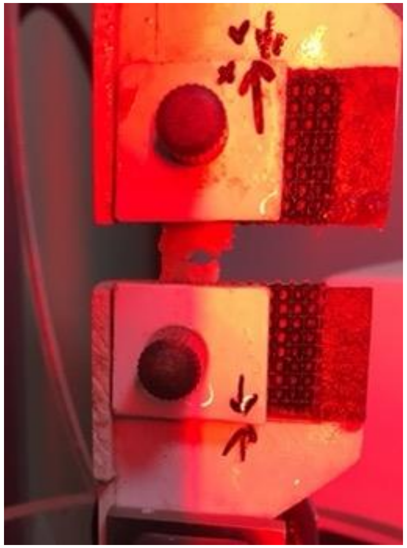

Visible gap reached during the test

Preconditioning testing of aorta samples

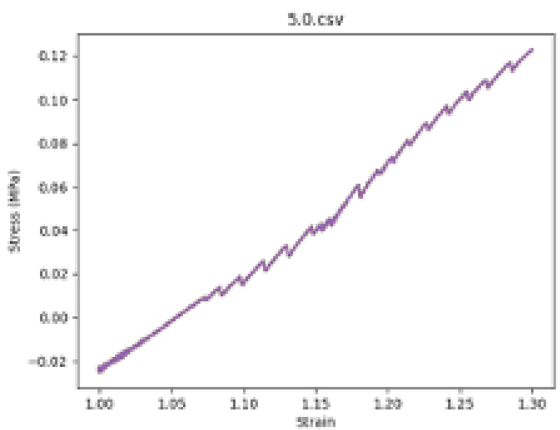

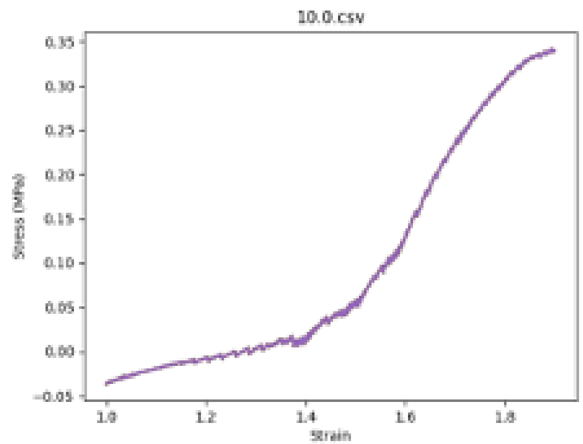

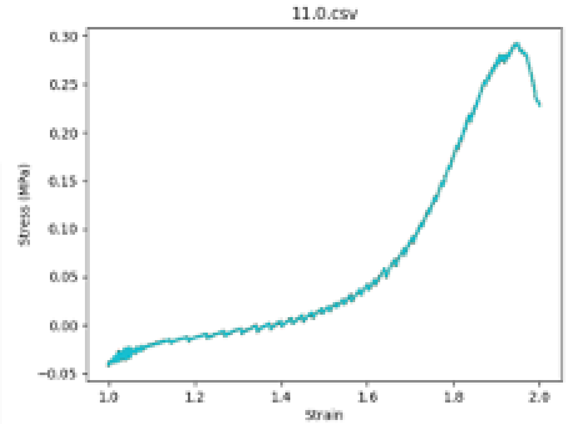

relative deformation growth from test to test, 2 attempts per each deformation value were performed

Critical mechanics data vs patient data

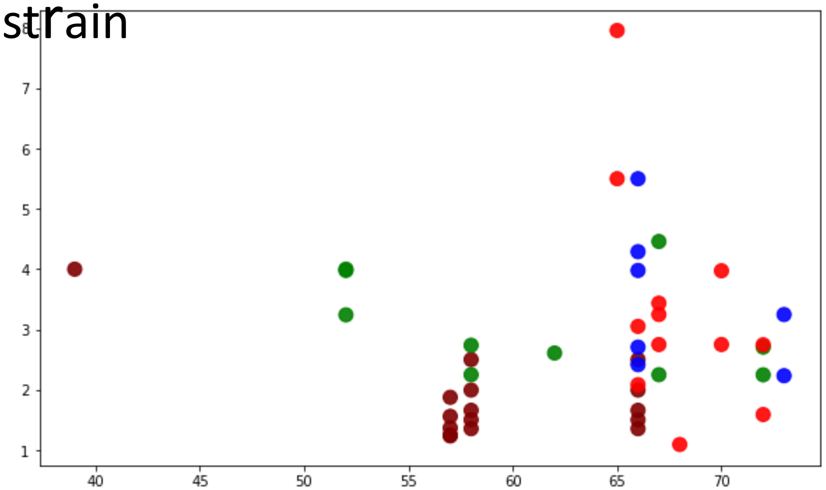

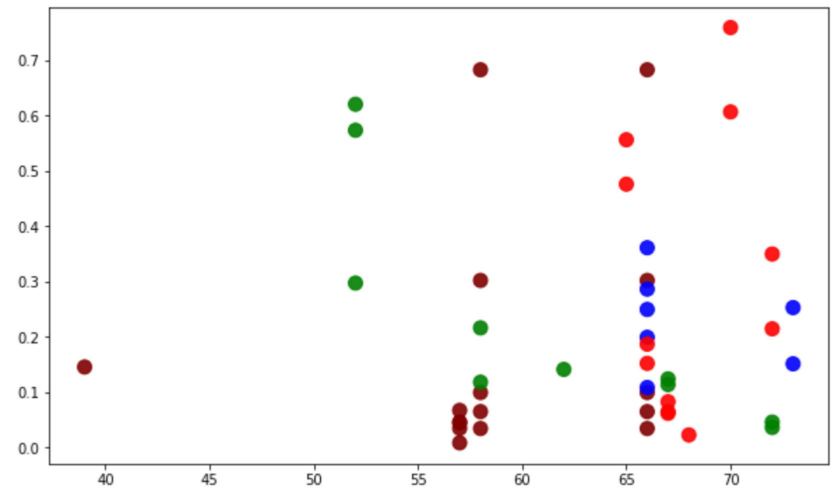

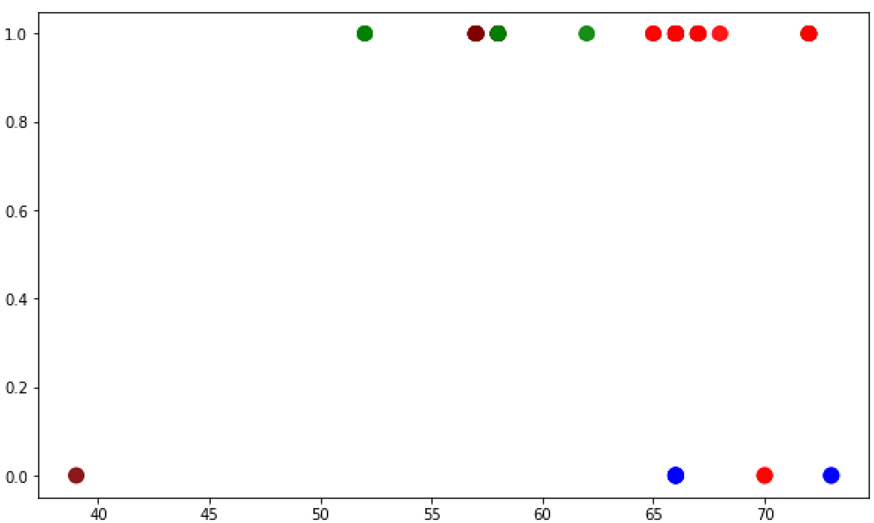

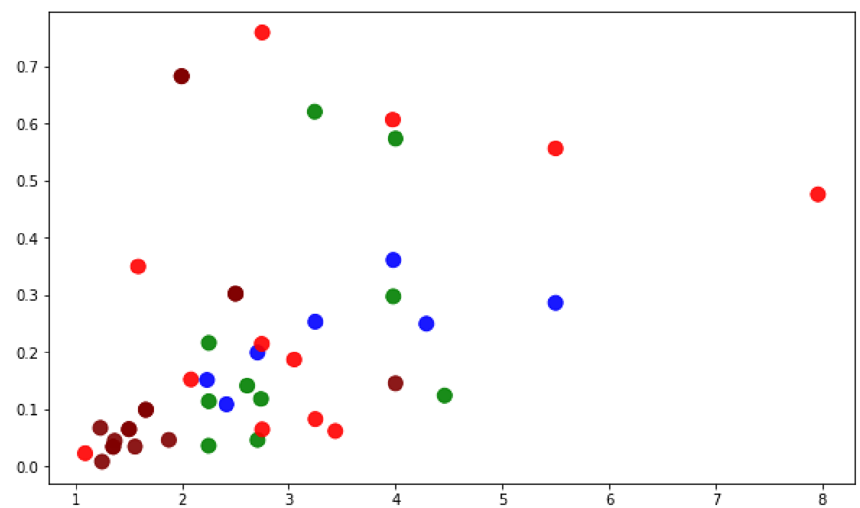

Proof of the remodeling of the AAA tissue

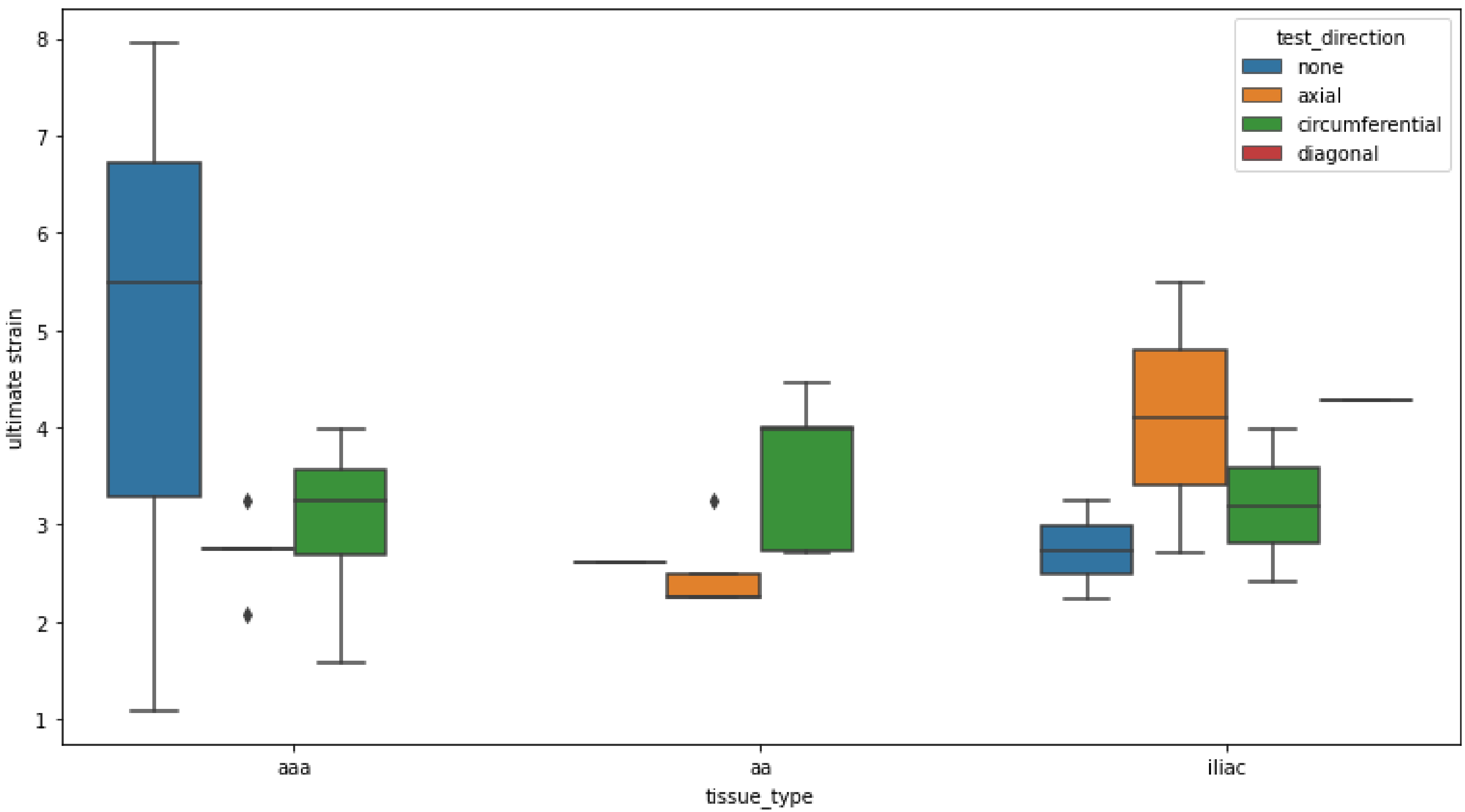

Proof of the remodeling of the AAA tissue

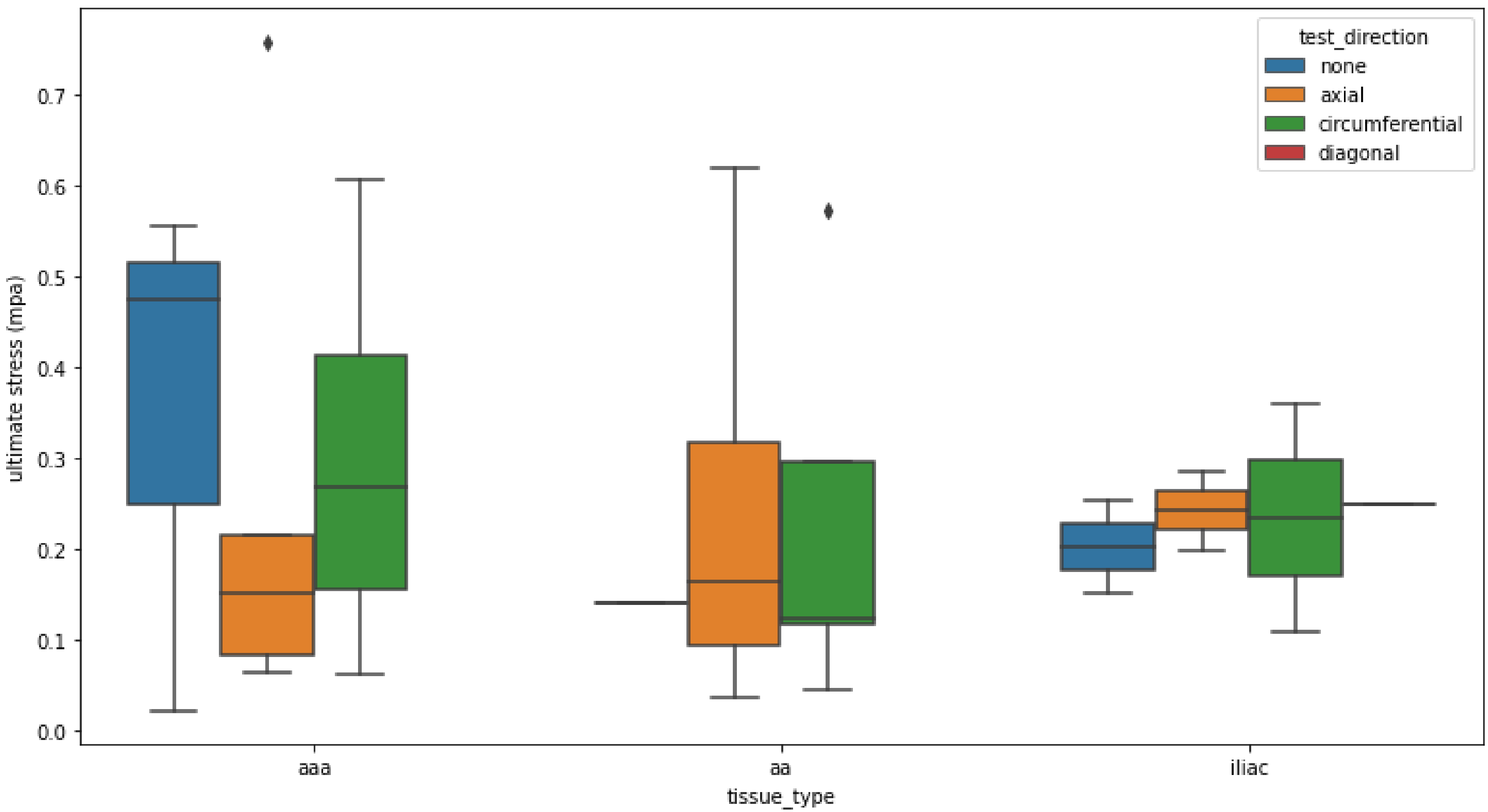

Thank you for your attention!

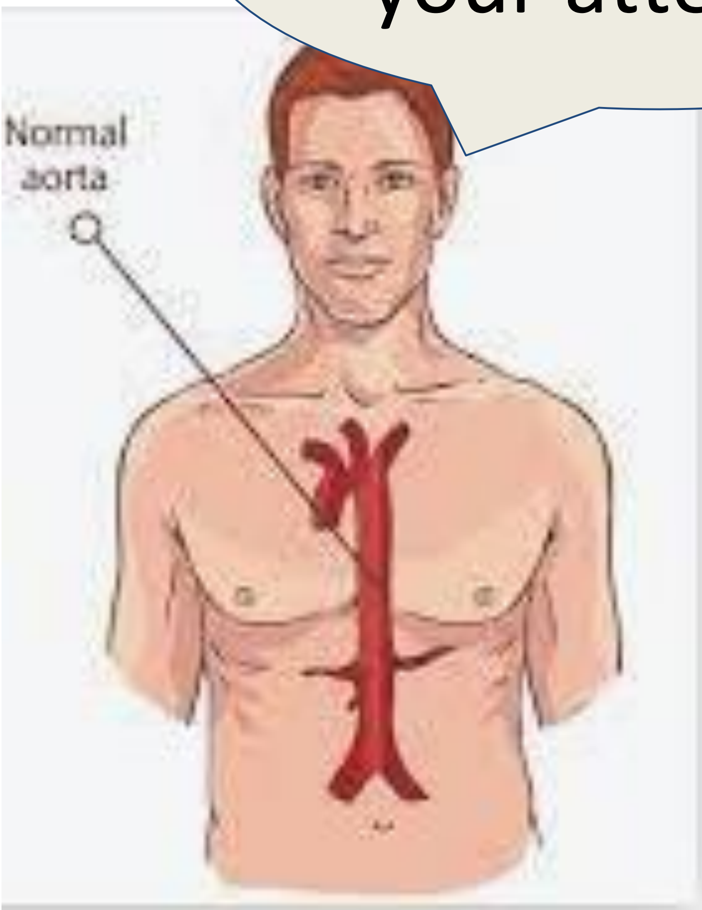

Partly supported by a grant from RSF 21-15-00091
Partly supported by a grant from RSF 20-71-10034
Team thanks LIH SB RAS for sharing ANSYS 2020R2 facilities